THE CONTINUOUS SPECTRA OF RADIO SOURCES

WITH PARTICULAR REFERENCE TO

NON-THERMAL GALACTIC SOURCES

Thesis by

Daniel E. Harris

In Partial Fulfillment of the Requirements

For the Degree of

Doctor of Philosophy

California Institute of Technology

Pasadena, California

1961

Acknowledgments

The observations on which this paper are based were made at the Owens Valley Radio Observatory of the California Institute of Technology, which is supported by the U. S. Office of Naval Research under Contract Nonr 220(19). It is a pleasure to thank our former director, J. G. Bolton, for his guidance; G. J. Stanley, acting director, who was responsible for the receiver and who critically read this manuscript; J. A. Roberts and K. I. Kellermann, who collaborated on Part I; and the staff and graduate students who helped in obtaining the observations.

A large section of the present work would have been impossible without a manuscript of the Manchester work on the Cygnus Loop, for which I am deeply indebted to D. Mathewson. I would also like to express my thanks to G. Westerhout, who kindly sent me flux densities of several sources at 400 Mc. The last section draws extensively on two recent papers by I. S. Shklovsky, and I would like to thank the Consultants Bureau, Inc. for making translations of these papers available to me in advance of publication.

Several other individuals have been very helpful in the course of this work. In particular, I would like to thank R. Minkowski for his pertinent suggestions and his generosity in putting plates at my disposal.

The Institute provided financial assistance in the form of tuition scholarships.

Abstract

960 Mc observations of over 400 sources are reported in two parts. Part I contains position and intensity measurements of 106 sources (chiefly taken from the recent Cambridge surveys), and the results of 376 intensity measurements of sources previously observed at Sydney. Spectral indices are derived from the intensity measurements and the previous investigator's observations. The resulting spectral index distribution has a median value of -0.65 ± 0.10 and a dispersion such that 75% of the values lie within 0.25 of the median. Galactic sources show a larger dispersion of spectral index than do the sources assumed to be external galaxies.

Part II is based on 960 Mc observations of extended galactic nebulae, usually identified with supernova remnants. Contour diagrams of antenna temperature are presented for four of the larger objects. A detailed study of the Cygnus Loop shows that the radio emission is chiefly non-thermal, with a spectral index of -0.1 ± 0.1. An attempt to detect linear polarization places an upper limit of 30% for selected regions of the Cygnus Loop. Spectral indices ranging from -0.8 to +0.5 are derived for 12 other sources. Calculations show that the occurrence of optical synchrotron radiation is not ruled out by existing observations. An empirical relation between spectral index and physical size of supernova remnants suggests that the energy spectrum of relativistic particles flattens with age. A possible mechanism for this behavior is considered.

Table of Contents.

Introduction

In 1958 the nature of the larger part of the discrete radio sources was still unknown. In an effort to help resolve this problem, the Owens Valley Radio Observatory was designed to accurately measure the positions of known radio sources. Thus, the primary job of the observatory has been to obtain a positional accuracy such as to allow little or no ambiguity in the identifications of radio sources with optical objects. Part I of this thesis represents the first approach to this problem.

In its conception, this work was planned to measure positions with a single dish in preparation for the more accurate interferometer work which is now in progress. However, intensity measurements of all the sources observed became readily available from the position records and since most of the sources were taken from low frequency catalogues, spectral indices were derived.

A study of spectra provides a method of determining the nature of radio sources. The spectral index is a fundamental physical parameter of sources and, in addition to aiding in identification work, it provides information about the process of emission. Because of the importance of this type of data, and because the position measurements reported here have already been used in the interferometer observations, this thesis is oriented toward the study of radio spectra.

Since the present work is one of the first extensive lists of high frequency intensities for sources already observed at low frequencies, we are in a position to obtain

spectra for a large number of objects. The assumption of a constant spectral index for each source is still made. This restriction must be abandoned eventually, but it is pertinent to the present study where most of the spectra depend on intensity measurements at only two frequencies.

Part I contains the results of observations of 90 sources listed by the Cambridge group (Edge et al, 1959 and Elsmore et al, 1959), and several hundred sources previously observed at Sydney (Mills, Slee and Hill, 1958, 1960). The study of Cambridge sources is reported in a paper by Harris and Roberts and is included in its entirety. As no position measurements were attempted for the Sydney sources, only statistical information is presented on their spectra.

It is shown that the spectral index distribution for sources away from the galactic plane has a fairly narrow width, and that 75% of the sources lie within 0.25 of the median value. The galactic sources show a much wider distribution. If the spectral index is to be a useful parameter in distinguishing objects of different types, the range of values found must be significantly larger than the errors in measurement. The galactic sources exhibit such a dispersion of spectral index, and a meaningful interpretation of the spectra of these objects seems feasible. Part II is an attempt to make such an interpretation and, in particular, is a study of so called supernova remnants. These objects are generally defined as all extended galactic radio sources that are not H II regions. The emission process of H II re-

gions is fairly well understood and the observations available tend to corroborate predictions on the nature of the emission. Thus H II regions are omitted from the present study, and the more interesting, non-thermal galactic sources are the objects studied. It is hoped that if progress is made in the study of the emission process of this class of radio source, it will help clarify the non-thermal mechanisms of radio sources in general. If the causes responsible for the large spread of spectral indices in supernova remnants are isolated, then we may gain knowledge of the external sources which do not exhibit such a large dispersion.

Part I - Statistical Study of Radio Spectra

When accurate knowledge is unavailable for individual objects, it is sometimes worthwhile to treat a large collection of data statistically to learn something of the nature of the class of objects, rather than of the individual objects themselves. Moreover, when we learn the nature of the inherent distribution of a physical quantity, we can then interpret departures from the distribution.

This approach has been used in studying the spectra of radio sources. The accuracy of measuring spectral indices has reached the point where individual values are meaningful, and therefore it is important to know the inherent width and median value of the spectral index distribution. Part I attempts to answer this problem. Intensity measurements and their corresponding spectral implications are reported in two sections. First, northern sources are considered in a study of objects taken chiefly from the third Cambridge survey (Edge et al, 1959), and then intensities of southern sources are compared with the survey of Mills, Slee and Hill (1958). The results are mutually consistent, but disagree with the work of Whitfield (1957).

CALIFORNIA INSTITUTE OF TECHNOLOGY
RADIO OBSERVATORY
OWENS VALLEY, CALIFORNIA

REPRINT

RADIO SOURCE MEASUREMENTS AT 960 MC/S

D. E. HARRIS AND J. A. ROBERTS

California Institute of Technology Radio Observatory
Owens Valley, California

I. INTRODUCTION

The major surveys of radio sources made at meter wavelengths have shown a disquieting lack of agreement,[1] and an independent study of these sources using as simple an antenna as possible seems to be desirable. As a partial step in this direction, we report here a study of 106 radio sources made with one of the equatorially mounted 90-foot paraboloids of the Owens Valley Radio Observatory. This investigation was made at a frequency of 960 Mc/s.

The primary result of the study is a reliable catalogue of sources that will be used as a "finding list" for precise position measurements currently being undertaken with the two antennas operating as an interferometer. In addition, however, the results provide valuable information on the spectra of the sources, and have also been used in a search for optical counterparts to the sources.

Ninety of the objects observed were taken from the Third Cambridge Survey (3C),[2] which was kindly made available to us prior to its publication. The remaining 16 objects in the present list were either taken from other catalogues or were discovered in the course of the present investigation.

The equipment is briefly described in Section II, and in Sections III and IV the methods of determining the positions and intensities of the sources are outlined. In Section V suggested

Reprinted from the *Publications of the Astronomical Society of the Pacific*
(Vol. 72, No. 427, August 1960)

optical identifications are discussed, while Section VI is devoted to a consideration of the spectra of the sources. The positions, intensities, spectral indices, and other pertinent data for the 106 sources are collected in Table I, which will be found at the end of the article (p. 248).

II. EQUIPMENT

The 90-foot parabolic reflector was fed by a waveguide horn giving a tapered illumination that fell to approximately 10% at the edges of the reflector. The resulting main beam was nearly circular and 0°.8 wide between half-power points, while the first sidelobe was approximately 1% of the main beam.

The receiver was of the comparison type, switching at 400 cps between the horn and a reference load. Initially this reference was a second horn mounted near the focus but directed away from the reflector. Later a resistor immersed in liquid nitrogen was used. This latter arrangement was less sensitive to external interference and less affected by variation in ground radiation as the antenna was moved.

The rf switch was of the quarter-wave variety and used gold-bonded germanium diodes as the switching elements. Special impedance-transforming sections were included between both the switch and the crystal mixer, and the mixer and the first i.f. amplifier, to insure optimum signal-to-noise conditions. The switch, mixer, and i.f. amplifier were mounted together in a box immediately behind the horn. The rest of the receiver was located inside the base tower of the antenna.

No image rejection was employed, so that both sidebands were utilized. The intermediate frequency was initially 30 Mc/s, but was later reduced to 10 Mc/s. In each case the bandpass was approximately 8 Mc/s wide, and the output time constant used was from 1 to 20 sec. The noise temperature of the receiver, as measured with a discharge tube noise generator, was approximately 300° K when the intermediate frequency was 30 Mc/s, and 200° K when the intermediate frequency was 10 Mc/s. The combination of the rf switch and interconnecting cables added approximately 90° K to the system temperature.

III. POSITION MEASUREMENTS

The apparent right ascension of a source was measured from a drift curve made with the antenna stationary and set on the 3C declination. From this record we determined the right ascension of a point midway between positions on either side of the source maximum and having equal amplitudes above a straight baseline of best fit (Figure 1*c*). Several such determinations were made

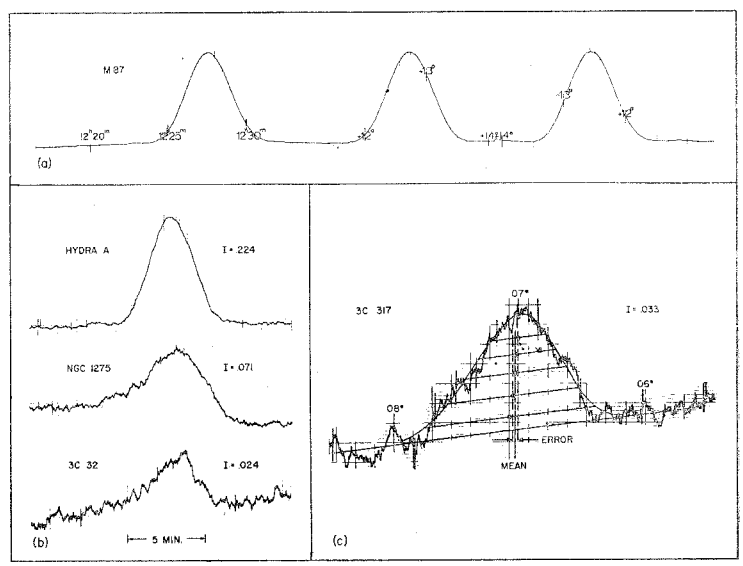

FIG. 1.—(*a*), Form of records used for position measurements. A drift curve is followed by two records made with the antenna tracking the source while being driven north and south at a rate of 1° in four minutes. (*b*), Examples of records used for intensity measurements showing the signal to noise ratio. The source intensity relative to M 87 is shown in the figure. The time constant was 20ˢ in all cases. (*c*), Method of analyzing the records for source position.

using points of different amplitude, and the mean of these was taken as the right ascension of the source. A reading error was assessed from the scatter of the individual determinations and was chosen so as to include approximately three-quarters of the points.

The declination was derived in a similar way from records made with the antenna tracking the correct right ascension while being driven in declination (both north and south) at a rate of 1° in four minutes.

The observed positions were corrected for refraction, precession, and errors in the telescope dials. These dial errors were determined each night by observing at least four of the five standard sources: the Crab Nebula, the Orion Nebula, M 87, Cygnus A and Cassiopeia A. These were chosen as position calibrators because of their strength, known optical position, and distribution over the sky. The dial errors for both right ascension and declination were found to be slow functions of declination; the right-ascension error varied by a total of $\sim 15^s$ and the declination error by $\sim 5'$ over the 65° range of declination covered by the calibrators.

The error assigned to a position observation was assessed as the sum of the reading error referred to above and an error due to the uncertainty of interpolation in the dial correction curves. Sources south of $\delta = -10°$ suffer from an additional uncertainty due to the lack of calibrators, and the estimates of error for these sources have been increased accordingly. Usually two or three observations were obtained for each source, and the quoted error is estimated from the individual errors and the extent of agreement among the observations. It is felt that the probability of finding a source within the quoted error limit is about 80%.

IV. INTENSITY MEASUREMENTS

Intensities were measured by setting the antenna at the declination of the source and about 12^m ahead in right ascension and noting the deflection of the output recorder as the source drifted through the antenna beam. For most of the sources the declination used was determined from the observations described in Section III. However, for a number of the weaker sources, position measurements were not made and the Cambridge declination was used. Figure 1*b* shows examples of the drift curves from which the intensity measurements were made.

All source intensities were measured relative to M 87 (Vir-

go A), which is one of the standard sources recommended by the I.A.U. and which was available during the night for the larger part of the program. During that part of the year when M 87 was not available at night, secondary calibrators, Cygnus A and the Crab Nebula, were used. Absolute measurements were not attempted and where flux densities are quoted in this paper they are based on an assumed value for M 87 of 300×10^{-26} watts $m^{-2}(c/s)^{-1}$. This value was derived from published spectral data.[3,4] Other estimates of the flux from M 87 were made from the measured ratio to Cassiopeia A and its published spectrum, from the measured ratio to the moon, assumed to be at a temperature of 250° K, and from an estimate of the receiver noise and antenna efficiency. These methods all gave figures consistent with the above value. Flux densities are included in Table I on the basis of this figure, but it should be borne in mind that the intensity relative to M 87 is our observed quantity.

The intensity ratios given in Table I are average values from several observations and the quoted errors are estimated such that about three-quarters of the individual values lie within the limits of error. Thus, these errors are a measure of internal consistency and do not encompass systematic errors. One possible cause of systematic error is the use of a wrong declination for sources whose position we did not measure.

For all but the strongest sources the deflection of the output meter was proportional to the input power. However, for Cassiopeia A, Cygnus A, and the Crab Nebula the antenna temperatures were comparable with the receiver temperature so that departures of the detector characteristic from a square law became important. Correction factors for these sources were determined by measuring the detector law with a variable-precision attenuator inserted between the two i.f. amplifiers. As a check on this method, a further series of observations of these sources was made with a fixed attenuator inserted between the horn and the rf switch, and with the nitrogen load replaced by a reference at ambient temperature. This arrangement increased the receiver temperature and reduced the effective antenna temperatures of these sources to such an extent that the detector law was unimportant.

The final intensity ratios for the strongest sources are weighted means of all the observations and are believed to be accurate to 5%.

V. OPTICAL FIELDS

The plates of the National Geographic Society–Palomar Observatory Sky Survey were examined in a search for optical counterparts to the sources listed in Table I. For this purpose use was made of all available data on the radio sources, including preliminary measurements with the two 90-foot antennas operating as an interferometer. Details of this work, which is still continuing, will be published later. We have included in Table I an indication of the nature of the optical field in the neighborhood of the source, and in the cases of possible identification some details are given in the notes to Table I.

The nature of the optical field near each source is indicated in Table I by the Roman numerals I to IV in the final column. These symbols have the following significance:

I. A prominent or isolated extragalactic object near the radio position (possible identification).

IIa. Several bright objects within the limits of error: a more accurate position ($\pm 0.^{\prime}5$) could lead to an identification.

IIb. Several bright objects so close together that positional accuracy better than $\pm 0.^{\prime}5$ would be required to make an identification.

III. Only faint objects near the position.

IV. Heavy absorption in the region; no galaxies visible.

Many of the class I objects have been discussed previously by Minkowski[5,6] or by Dewhirst.[1,2,7]

VI. SPECTRA

By comparing the source intensities measured in the present investigation with those reported in the Cambridge surveys at 159 or 178 Mc/s,[2,7]* we obtained special information for the 90

* We wish to thank Drs. Elsmore, Ryle, and Leslie for communicating their results to us in advance of publication.

sources common to the two programs. The data were fitted to an assumed spectrum of the form

$$\text{flux density} \propto (\text{frequency})^{x},$$

where x is termed the spectral index. As the present intensities were measured relative to M 87, the spectral indices quoted in Table I are those relative to M 87, i.e., they are $x - x_{\text{M 87}}$. The spectral index of M 87 itself has been given as -0.74 by Whitfield,[3] and the 3C and Elsmore *et al.* values for the flux of M 87, taken in conjunction with our adopted 960 Mc/s value, yield indices of -0.72 and -0.70, respectively.

The distribution of the 90 values of the relative spectral index is shown in Figure 2*a*. There is seen to be a close clustering about the median value of $+0.1$ (a spectrum slightly flatter than that of M 87). About 10% of the values form a tail on the positive side, corresponding to spectra that are flatter than that of M 87, or increase with frequency.

At the other extreme, the steepest spectrum measured had an index relative to M 87 of -0.5, or an absolute spectral index of ~ -1.2. This is contrary to the conclusions of Whitfield, who found that 25% of the sources he studied had spectral indices steeper than -1.2 and that a few were as extreme as -1.8.[3] All but one of these sources are included in the present study. Provided only that the source spectra follow approximately a power law, it seems that the present indices, based on intensities at two widely spaced frequencies, will be subject to considerably less error than those derived by Whitfield, which often were based on intensities at a few closely spaced frequencies. For this reason we believe that the distribution of spectral indices shown in Figure 2*a* approaches the true distribution more closely than the distribution given by Whitfield.

The question then arises: How nearly does the present histogram approximate the true distribution and to what extent is it broadened by errors in the observations? In Figure 2*a*, 75% of the spectral indices lie within ± 0.25 of the median value. From the errors assigned to the two sets of observations one would expect a spread in which 75% of the spectral indices lay within ± 0.15 of their true value. This is sufficiently less than the ob-

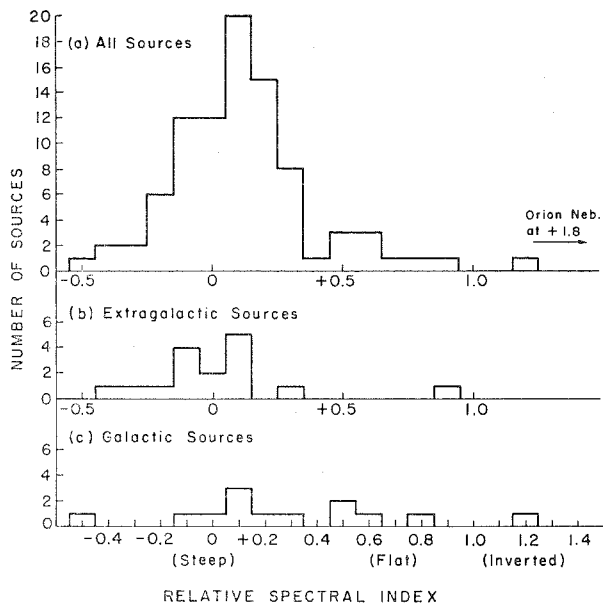

FIG. 2.—Histograms of relative spectral index ($x - x_{MST}$). (*a*), The 90 sources common to this paper and the recent Cambridge lists.[2,7] (*b*), The 5 well-known extragalactic sources, together with 11 probable identifications of galaxies (the Class I objects in Table I). (*c*), Galactic objects for comparison with (*b*). These sources include all objects in (*a*) that have $b \leqslant 10°$ and a diameter (Cambridge value) of 3′ or more, together with Kepler's supernova.

served spread to suggest that the errors do not broaden the observed distribution very markedly. This point was further tested by subdividing the data according to the magnitude of the errors in the flux measurements. For each of these subgroups the spread of the distribution obtained was substantially the same, again implying that the errors do not make a major contribution to the width of the observed distribution.

In a search for systematic differences in spectral index between different classes of objects, similar histograms were constructed with the sources grouped according to (1) intensity, (2) diameter (Cambridge data), and (3) galactic latitude. Although the group-

ing according to intensity suggests that the weaker sources may have slightly steeper spectra, the only grouping that yields a significant difference is the division into galactic and extragalactic objects. This separation is shown in the histograms of Figures 2*b* and 2*c*. Although the number of sources is too small for quantitative conclusions, the figures certainly suggest that the spectral indices of galactic objects are scattered over a much wider range than those of extragalactic objects. Thus all of the extragalactic spectral indices, except for 3C 270, lie within ± 0.35 of the index for M 87, and if the intensity given by Mills *et al.*[8] is used for 3C 270, its index also falls within this range.*

Those sources in Figure 2*a* having extreme spectral indices were studied in more detail. Of the eleven sources with relative spectral indices $> +0.45$ ("flatter" spectra), four are identified galactic sources whose spectrum is well established (the Orion Nebula, the Rosette Nebula, the Crab Nebula, and IC 443). For the other seven sources alternative indices were computed by using the present 960 Mc/s intensities in conjunction with either the 81.5 Mc/s intensities of the 2C survey,[9] the 85 Mc/s intensities of Mills *et al.*,[8] or the 169 Mc/s intensities of Boischot.[10] In most cases, these alternative values were $< +0.45$, suggesting that the measurements are confused in some way. However for 3C 58 and 3C 398 even the alternative values are $> +0.6$. As both of these sources lie close to the galactic plane and have diameters of several minutes of arc, they are very probably galactic objects.

Of the five sources with excessively steep spectra (relative index < -0.25), only for 3C 28 do the alternative values confirm the index (-0.4). However, in this case the 960 Mc/s intensity may be too low as the position of this source was not measured in the present program.

VII. CONCLUSIONS

This study has demonstrated the general reliability of the Third Cambridge Catalogue, and indirectly confirmed the (relative) intensities of that catalogue by the narrow range of spectral

* Preliminary Caltech diameter measurements suggest that the 3C intensity may be low because of partial resolution of the source.

indices deduced in Section VI. Only one 3C source (3C 442) was not found, although for 3C 382 and 3C 384 a single source was found at an intermediate position (an alternative suggested in the 3C catalogue). 3C 442 was later found one lobe north of the quoted 3C position. A detailed comparison of the positions reveals that of the 69 sources from the 3C catalogue whose positions were measured in the present program, only 46 (67%) agree within the sum of the errors. Most of the disagreements are in right ascension only. For about half of these cases of disagreement, the positions have also been measured by either Elsmore *et al.*[7] or Mills *et al.*[8] Their measurements did not consistently agree with either the 3C values or the present observations. The present study, in conjunction with the Cambridge survey, has also shown that the spectral indices of the majority of the sources lie within a surprisingly small range. The median index is approximately -0.6, and 80% of the values lie between -0.3 and -0.9 (Section VI). This result has an important bearing on theories of the generation of nonthermal radio emission. Under fairly general conditions for the synchrotron theory, it implies that the distribution of electron energies must be similar in all of the sources.

The classification of the optical fields given in Table I provides a useful indication of the sources for which more accurate position measurements are most likely to prove fruitful (classes I and II). Our examination of the 48-inch Schmidt plates supports the idea that extragalactic radio sources tend to be associated with elliptical galaxies, and particularly with double and multiple systems.[1]

This investigation formed part of the program of the Owens Valley Radio Observatory and was carried out under U.S. Office of Naval Research contract Nonr-220(19). We are grateful to Professor J. G. Bolton for his guidance and encouragement in this work; to Mr. G. J. Stanley, who was responsible for the receiving equipment; to Mr. B. G. Clark for his help in examining the Schmidt plates; and to our several colleagues for their assistance in the observational program.

[1] See, e.g., D. W. Dewhirst, in *Paris Symposium on Radio Astronomy*, R. N. Bracewell, ed. (Stanford, Calif.: Stanford University Press, 1959), p. 507.

[2] D. O. Edge, J. R. Shakeshaft, W. B. McAdam, J. E. Baldwin, and S. Archer, *Mem. R.A.S.*, **68**, 37, 1959.

[3] G. R. Whitfield, *M.N.R.A.S.*, **117**, 680, 1957.

[4] C. H. Seeger, U.R.S.I. Commission V, Report from Subcommission V*d*, June 1957.

[5] R. Minkowski, *Pub. A.S.P.*, **70**, 143, 1958.

[6] R. Minkowski, *Proc. Nat. Acad. Sci.*, **46**, 13, 1960.

[7] B. Elsmore, M. Ryle, and P.R.R. Leslie, *Mem. R.A.S.*, **68**, 61, 1959.

[8] B. Y. Mills, O. B. Slee, and E. R. Hill, *Aust. J. Phys.*, **11**, 360, 1958.

[9] J. R. Shakeshaft, M. Ryle, J. E. Baldwin, B. Elsmore, and J. H. Thomson, *Mem. R.A.S.*, **67**, 106, 1955.

[10] A. Boischot, in *Paris Symposium on Radio Astronomy*, R. N. Bracewell, ed. (Stanford, Calif.: Stanford University Press, 1959), p. 492.

[11] G. Westerhout, *B.A.N.*, **14**, 215, 1958 (No. 488).

[12] R. Hanbury Brown and C. Hazard, *M.N.R.A.S.*, **113**, 123, 1953.

[13] V. F. Gaze and G. A. Shaĭn, *Pub. Crimean Astrophysical Obs.*, **15**, 11, 1955.

[14] J. G. Bolton and B. G. Clark, *Pub. A.S.P.*, **72**, 29, 1960.

TABLE I

960 Mc/s Source List A

Source		Right Ascension			Declination		
No.	Name	(1950)	Δ	Pre-cession	(1950)	Δ	Pre-cession
1	N.P.C.	$00^h02^m35^s$	$\pm30^s$	$+3^s.14$	$+72°04'.5$	$\pm 4'$	$+0'.33$
2	SN 1572	00 22 45.7	± 3	+3.34	+63 51.4	± 1	+0.33
3	3C 15	00 34 24	±10	+3.07	−01 20	± 4	+0.33
4	3C 17	00 35 40	± 8	+3.06	−02 23	± 4	+0.33
5	3C 20	00 39 56	±16	+3.37	+51 47	± 2	+0.33
6	NGC 281	00 50 05	±12	+3.43	+56 20.4	± 1.5	+0.33
7	3C 27	00 53 20	±15	+3.85	+68 00	± 3	+0.33
8	3C 28	(00 53 09.9	± 1)	+3.22	(+26 08.8	± 1)	+0.33
9	3C 32	01 05 47	±10	+2.96	−16 19.8	± 2*	+0.32
10	3C 33	01 06 21	± 5	+3.16	+13 06	± 3	+0.32
11	3C 38	01 18 05	±12	+2.95	−15 44	± 6	+0.32
12	3C 40	01 23 20	± 4	+3.06	−01 37.7	± 2	+0.31
13	3C 41	01 24 22	± 6	+3.38	+32 55	± 4	+0.31
14	3C 47	01 33 45	± 6	+3.22	+20 47	± 5	+0.31
15	3C 48	01 34 45	± 8	+3.42	+32 54.6	± 1.5	+0.31
16	3C 58	02 01 45	± 5	+4.50	+64 35.8	± 1.5	+0.29
17	3C 63	02 18 07	±10	+3.05	−02 12	± 6	+0.28
18	3C 66	02 19 49	± 4	+3.78	+42 45	± 3	+0.27
19	3C 75	02 54 55	± 6	+3.16	+05 53	± 3	+0.24
20	3C 79	03 07 07	± 8	+3.37	+16 54	± 2	+0.23
21	N.P.C.	03 16 22	±15	+3.28	+16 18.5	± 4	+0.23
22	NGC 1275	03 16 27	± 6*	+3.96	+41 21.3	± 1.5*	+0.22
23	Fornax A	03 20 25	±15	+2.30	−37 21.5	± 4	+0.22
24	3C 86	03 23 05	±15	+4.56	+55 06.8	± 2	+0.21
25	3C 89	03 31 26	±10	+3.05	−01 25	±10	+0.20
26	N.P.C.	03 36 54	±50*	+3.07	−01 55	± 8*	+0.19
27	3C 98	03 56 00	±10	+3.35	+10 19.7	± 2	+0.17
28	3C 103	04 04 39	±10	+4.18	+42 51.3	± 2.5	+0.16
29	3C 109	04 11 00	±15	+3.31	+11 07	± 4	+0.15
30	3C 111	04 15 06	± 8	+4.01	+37 53.3	± 1	+0.15
31	3C 123	04 33 50	± 3	+3.78	+29 34.1	± 1	+0.12
32	3C 129	04 45 40	±14*	+4.34	+44 56.4	± 4*	+0.11
33	HB 9	04 57 30	±30	+4.43	+46 26	± 4	+0.09
34	3C 134	05 01 12	±10*	+4.08	+38 00	± 4*	+0.09
35	Pictor A	05 18 19	±10	+1.72	−45 52	± 5	+0.06

TABLE I

960 Mc/s Source List A

No.	Intensity: Ratio to M 87	Intensity: [10^{-26} watts m^{-2} $(c/s)^{-1}$]	Relative Spectral Index	Optical Field
1	.043 ± .005	12.9 ± 1.5		
	(.25 ± .06)	(75 ± 18)		
2	.19 ± .01	57 ± 3	+0.19 ± 0.08	
3	.017 ± .004	5.1 ± 1.2	−0.06 ± 0.18	III
4	.034 ± .008	10.2 ± 2.4	+0.32 ± 0.26	IIa
5	.045 ± .005	13.5 ± 1.5	+0.13 ± 0.11	IV
6	.052 ± .004	15.6 ± 1.2		
	(.059 ± .006)	(17.7 ± 1.8)		
7	.036 ± .005	10.8 ± 1.5	+0.33 ± 0.17	IV
8	.008 ± .003	2.4 ± 0.9	−0.45 ± 0.22	IIb
9	.024 ± .005	7.2 ± 1.5	+0.16 ± 0.19	IIa
10	.060 ± .002	18 ± 0.6	+0.11 ± 0.07	I
11	.028 ± .005	8.4 ± 1.5	+0.19 ± 0.17	III
12	.027 ± .006	8.1 ± 1.8	+0.07 ± 0.20	I
13	.023 ± .003	6.9 ± 0.9	+0.59 ± 0.17	III
14	.021 ± .003	6.3 ± 0.9	−0.07 ± 0.16	IIa
15	.071 ± .006	21.3 ± 1.8	+0.28 ± 0.10	III
16	.111 ± .005	33.3 ± 1.5	+1.24 ± 0.15	IV
17	.020 ± .003	6.0 ± 0.9	+0.10 ± 0.13	III
18	.043 ± .003	12.9 ± 0.9	+0.30 ± 0.14	I
19	.025 ± .002	7.5 ± 0.6	+0.02 ± 0.10	I
20	.023 ± .002	6.9 ± 0.6	−0.09 ± 0.10	III
21	.030 ± .003	9.0 ± 0.9		III
22	.071 ± .007	21.3 ± 2.1	+0.06 ± 0.11	
23	.41 ± .02	123 ± 6		
	(.50 ± .04)	(150 ± 12)		
24	.040 ± .003	12 ± 0.9	+0.25 ± 0.10	IV
25	.021 ± .003	6.3 ± 0.9	+0.09 ± 0.18	IIa
26	.012 ± .004	3.6 ± 1.2		III
27	.047 ± .004	14.1 ± 1.2	+0.10 ± 0.10	I
28	.022 ± .002	6.6 ± 0.6	−0.18 ± 0.10	IV
29	.017 ± .003	5.1 ± 0.9	−0.03 ± 0.16	III
30	.068 ± .005	20.4 ± 1.5	+0.08 ± 0.09	IV
31	.215 ± .006	64.5 ± 1.8	+0.10 ± 0.07	IV
32	.031 ± .004	9.3 ± 1.2	−0.02 ± 0.12	III
33	.075 ± .015	22.5 ± 4.5		
	(.53 ± .10)	(160 ± 30)		
34	.050 ± .004	15.0 ± 1.2	−0.16 ± 0.10	IV
35	.280 ± .020	84 ± 6		

TABLE I (*Continued*)

Source		Right Ascension			Declination		
No.	Name	(1950)	Δ	Pre-cession	(1950)	Δ	Pre-cession
36	Crab Nebula	$05^h31^m30^s$		+3ˢ16	+21°59′.3		+0′.04
37	Orion Nebula	05 32 49		+2.94	−05 25.3		+0.04
38	S 147	05 36		+3.78	+28		+0.03
39	3C 147	05 38 44	± 6ˢ	+4.65	+49 47	± 3′	+0.03
40	3C 154	06 10 23	±20*	+3.72	+26 03	± 7*	−0.01
41	IC 443	06 14 16	± 6*	+3.64	+22 36.4	± 3*	−0.02
42	3C 161	06 24 37	±10	+2.93	−05 51.4	± 2	−0.04
43	Rosette Nebula	06 29 24	±10	+3.19	+04 53	± 3	−0.04
44	3C 171	06 51 10	±15	+4.87	+54 12.4	± 2	−0.07
45	3C 196	08 10 02	±12	+4.34	+48 23	± 4	−0.18
46	Puppis A	08 21 20	±15	+2.06	−42 52	± 4	−0.19
47	Hydra A	09 15 43	± 2	+2.89	−11 52.4	± 1	−0.25
48	3C 227	09 44 59	± 8*	+3.17	+07 39	± 6*	−0.28
49	3C 234	09 58 26	±10*	+3.45	+29 02.4	± 4*	−0.29
50	3C 237	(10 05 21.9	± 1.5)	+3.16	(+07 43.8	± 2)	−0.29
51	3C 264	(11 42 34	± 6)	+3.11	(+20 00	± 9)	−0.33
52	3C 270	12 16 49	± 5	+3.06	+06 06	± 3	−0.33
53	3C 273	12 26 40	± 6	+3.07	+02 20	± 2	−0.33
54	M 87	12 28 18		+3.04	+12 40.1		−0.33
55	3C 278	(12 52 00	± 6)	+3.14	(−12 25	± 6)	−0.33
56	3C 279	(12 53 37	± 3)	+3.10	(−05 41	± 7)	−0.33
57	3C 280	(12 54 41.9	± 0.5)	+2.73	(+47 35.3	± 1)	−0.33
58	3C 283	13 08 50	±18*	+3.24	−22 11	± 5*	−0.32
59	NGC 5128	(13 22 28)		+3.51	(−42 45.6)		−0.31
60	3C 286	(13 28 49.7	± 1.5)	+2.77	(+30 45.6	± 1.5)	−0.31
61	3C 287	(13 29 04	± 3)	+2.82	(+25 24	± 6)	−0.31
62	3C 295	14 09 35	±12	+2.14	+52 25	± 3*	−0.28
63	3C 298	14 16 36	±12*	+2.98	+06 46	± 4*	−0.28
64	3C 310	15 02 30	±12*	+2.60	+26 12.5	± 2*	−0.23
65	3C 313	15 08 12	± 9*	+2.98	+08 03	± 4*	−0.23
66	3C 315	15 11 29	±10*	+2.58	+26 21	± 9*	−0.22
67	3C 317	15 14 14	±12	+2.95	+07 10	± 3	−0.22
68	3C 318	(15 17 52	± 6)	+2.69	(+20 28	± 5)	−0.22
69	3C 324	(15 47 34	± 5)	+2.63	(+21 33	± 7)	−0.18
70	3C 327	15 59 57	± 6*	+3.03	+02 04.6	± 3*	−0.17

TABLE I (*Continued*)

No.	Intensity: Ratio to M 87	Intensity: [10^{-26} watts m^{-2} $(c/s)^{-1}$]	Relative Spectral Index	Optical Field
36	3.43 ± .15	1030 ± 45	+0.51 ± 0.08	
37	1.20 ± .03	360 ± 9	+1.88 ± 0.06	
38	.043 ± .005	12.9 ± 1.5		
	(.4 ± .2)	(120 ± 60)		
39	.097 ± .003	29.1 ± 0.9	+0.25 ± 0.07	IV
40	.023 ± .002	6.9 ± 0.6	+0.18 ± 0.11	IV
41	.43 ± .02	129 ± 6	+0.54 ± 0.12	
	(.65 ± .08)	(195 ± 24)		
42	.080 ± .005	24.0 ± 1.5	+0.14 ± 0.09	IV
43	.350 ± .006	105 ± 2	+0.57 ± 0.20	
	(1.14 ± .12)	(342 ± 36)		
44	.020 ± .003	6.0 ± 0.9	+0.06 ± 0.18	III
45	.070 ± .005	21.0 ± 1.5	+0.02 ± 0.09	IIa
46	.34 ± .02	102 ± 6		
	(.44 ± .04)	(132 ± 12)		
47	.224 ± .006	67.2 ± 1.8	+0.09 ± 0.09	
48	.034 ± .003	10.2 ± 0.9	+0.07 ± 0.10	IIb
49	.024 ± .003	7.2 ± 0.9	−0.11 ± 0.12	IIb
50	.018 ± .003	5.4 ± 0.9	−0.09 ± 0.14	III
51	.035 ± .010	10.5 ± 3.0	+0.18 ± 0.20	IIa
52	.095 ± .005	28.5 ± 1.5	+0.93 ± 0.19	I
53	.167 ± .008	50.1 ± 2.4	+0.47 ± 0.15	III
54		300	0.00 ± 0.08	
55	.032 ± .005	9.6 ± 1.5	−0.10 ± 0.19	I
56	.023 ± .004	6.9 ± 1.2	+0.11 ± 0.18	III
57	.023 ± .004	6.9 ± 1.2	−0.02 ± 0.15	III
58	.034 ± .005	10.2 ± 1.5	+0.02 ± 0.19	III
59	1.54 ± .10	462 ± 30		
	(6.7 ± .5	(2010 ±150)		
60	.065 ± .005	19.5 ± 1.5	+0.62 ± 0.09	III
61	.028 ± .004	8.4 ± 1.2	+0.04 ± 0.18	III
62	.102 ± .008	30.6 ± 2.4	+0.19 ± 0.10	III
63	.037 ± .005	11.1 ± 1.5	−0.08 ± 0.13	III
64	.036 ± .006	10.8 ± 1.8	−0.28 ± 0.14	I
65	.018 ± .003	5.4 ± 0.9	−0.32 ± 0.14	III
66	.020 ± .003	6.0 ± 0.9	−0.10 ± 0.21	I
67	.033 ± .003	9.9 ± 0.9	−0.16 ± 0.10	IIa
68	.009 ± .003	2.7 ± 0.9	−0.20 ± 0.24	III
69	.021 ± .005	6.3 ± 1.5	+0.12 ± 0.24	III
70	.039 ± .007	11.7 ± 2.1	−0.03 ± 0.14	IIa

TABLE I (*Concluded*)

Source		Right Ascension			Declination		
No.	Name	(1950)	Δ	Precession	(1950)	Δ	Precession
71	3C 330	$16^h09^m05^s$	±20^s	+0^s.40	+66°05′	± 3′	−0′.16
72	3C 338	16 26 54	±10	+2.06	+39 35.3	± 2.5	−0.13
73	3C 343	16 36 56	±14*	+0.65	+62 41.7	± 2.5	−0.12
74	3C 345	16 41 57	± 5	+2.02	+39 53.5	± 2	−0.11
75	Hercules A	16 48 43	± 2	+2.96	+05 06.4	± 0.5	−0.10
76	3C 353	17 17 59	± 3	+3.05	−00 55.5	± 1.5	−0.06
77	MSH 17−16	(17 19 24	±30)	+3.52	(−18 45	± 7)	−0.06
78	SN 1604	(17 27 47	± 5)	+3.58	(−21 16	±10)	−0.05
79	3C 380	18 28 17	± 8	+1.56	+48 41	± 2	+0.04
80	N.P.C.	18 33 21	± 6	+2.22	+32 40.6	± 1	+0.05
81	3C 386	18 36 13	± 8	+2.75	+17 05.5	± 2	+0.05
82	3C 388	18 42 31	± 9	+1.74	+45 28	± 3	+0.06
83	3C 392	(18 53 35	± 5)	+3.05	(+01 15	± 7)	+0.07
84	3C 398	(19 08 44.4	± 1.5)	+2.87	(+09 05	± 4)	+0.10
85	3C 401	19 40 21	±20	+0.92	+60 33.4	± 3	+0.14
86	3C 402	(19 40 23	± 7)	+1.60	(+50 32	± 8)	+0.14
87	3C 403	19 49 38	±16	+3.03	+02 21.7	± 2	+0.15
88	Cygnus A	19 57 44.5		+2.08	+40 35.8		+0.16
89	3C 409	20 12 18	±10*	+2.59	+23 25	± 3*	+0.18
90	3C 410	20 18 01	±15	+2.45	+29 33.5	± 1	+0.19
91	HB 21	20 45		+1.85	+50 30		+0.22
92	3C 424	(20 45 43	± 4)	+2.95	(+06 50	± 6)	+0.22
93	Cygnus Loop	20 50		+2.50	+30		+0.23
94	3C 430	21 16 34	± 8	+1.52	+60 36	± 1.5	+0.25
95	3C 433	21 21 30	±10	+2.68	+24 50.3	± 3	+0.26
96	3C 436	21 42 01	±10	+2.67	+27 54	± 6	+0.28
97	N.P.C.	21 51 37	± 7*	+2.30	+46 50	± 3*	+0.28
98	3C 438	21 53 54	± 6	+2.53	+37 43.4	± 2	+0.28
	3C 442	(22 10 30	± 4)	+2.95	(+10 50	± 6)	+0.30
99	3C 444	22 11 33	± 8	+3.26	−17 13.7	± 3	+0.29
100	3C 445	22 21 17	±12	+3.10	−02 27	± 4	+0.30
101	3C 446	22 23 03	±10	+3.13	−05 14.6	± 3	+0.30
102	N.P.C.	22 29 53	± 6	+2.97	+11 28.2	± 2	+0.31
103	3C 452	22 43 33	±10	+2.71	+39 25	± 3	+0.32
104	3C 459	23 13 57	± 6	+3.05	+03 49	± 3	+0.33
105	Cassiopeia A	23 21 11.4		+2.71	+58 31.9		+0.33
106	3C 465	23 35 53	± 8	+3.00	+26 46.3	± 3	+0.33

TABLE I (*Concluded*)

No.	Intensity: Ratio to M 87	Intensity: [10^{-26} watts m^{-2} $(c/s)^{-1}$]	Relative Spectral Index	Optical Field
71	.029 ± .005	8.7 ± 1.5	+0.15 ± 0.15	III
72	.024 ± .004	7.2 ± 1.2	−0.37 ± 0.14	I
73	.035 ± .003	10.5 ± 0.9	+0.43 ± 0.12	III
74	.028 ± .004	8.4 ± 1.2	+0.70 ± 0.15	IIa
75	.245 ± .020	73.5 ± 6	−0.19 ± 0.10	
76	.279 ± .006	83.7 ± 1.8	+0.17 ± 0.06	III
77	.017 ± .006	5.1 ± 1.8		IV
	(.12 ± .08)	(36 ± 24)		
78	.065 ± .007	19.5 ± 2.1	+0.12 ± 0.15	
79	.061 ± .002	18.3 ± 0.6	+0.03 ± 0.07	III
80	.023 ± .002	6.9 ± 0.6		IIa
81	.032 ± .002	9.6 ± 0.6	+0.17 ± 0.09	III
82	.033 ± .004	9.9 ± 1.2	+0.28 ± 0.13	III
83	.703 ± .030	211 ± 9	+0.29 ± 0.08	IV
84	.30 ± .06	90 ± 18	+0.85 ± 0.16	IV
85	.026 ± .003	7.8 ± 0.9	+0.15 ± 0.13	III
86	.015 ± .004	4.5 ± 1.2	+0.04 ± 0.22	IIa
87	.032 ± .002	9.6 ± 0.6	+0.23 ± 0.15	IV
88	7.2 ± .4	2160 ±120	−0.09 ± 0.08	
89	.073 ± .004	21.9 ± 1.2	−0.03 ± 0.08	IV
90	.043 ± .003	12.9 ± 0.9	+0.07 ± 0.13	IV
91	.20 ± .02	60 ± 6		
	(.6 ± .2)	(180 ± 60)		
92	.021 ± .003	6.3 ± 0.9	+0.22 ± 0.19	III
93	.11 ± .01	33 ± 3		
	(.84 ± .15)	(252 ± 45)		
94	.037 ± .005	11.1 ± 1.5	−0.50 ± 0.24	III
95	.051 ± .005	15.3 ± 1.5	−0.07 ± 0.11	I
96	.021 ± .002	6.3 ± 0.6	+0.06 ± 0.13	IV
97	.015 ± .002	4.5 ± 0.6		IV
98	.035 ± .002	10.5 ± 0.6	−0.16 ± 0.09	IV
	not detected			
99	.045 ± .002	13.5 ± 0.6	+0.02 ± 0.12	IIa
100	.027 ± .004	8.1 ± 1.2	+0.15 ± 0.13	IIa
101	.026 ± .003	7.8 ± 0.9	+0.29 ± 0.12	III
102	.024 ± .002	7.2 ± 0.6		IIa
103	.046 ± .003	13.8 ± 0.9	−0.09 ± 0.09	III
104	.024 ± .002	7.2 ± 0.6	+0.02 ± 0.14	III
105	10.4 ± .5	3120 ±150	−0.05 ± 0.08	
106	.039 ± .003	11.7 ± 0.9	+0.08 ± 0.10	IIa

NOTES TO TABLE I

The first column lists a serial number and the second column gives the source name. The sources are usually designated by the 3C number, except where a more common term such as the optical name is well known. Sources not previously catalogued are indicated by "N.P.C.," except for unquestionable identifications such as NGC 281. It is suggested that N.P.C. sources be referred to as "CTA" followed by the serial number. "CT" is an abbreviation for "Caltech" and the letter "A" denotes the first list of radio sources published by this observatory.

The next six columns give the position of the source together with the estimated errors (Δ) and the annual precession. An asterisk indicates that the value is the result of a single observation. Positions in parentheses are those given by the previous observer and indicate that no measurement of position was made in the present study.

The intensity is tabulated both as a ratio to M 87 and as a flux density based on a value of 300×10^{-30} watts $m^{-2}(c/s)^{-1}$ for M 87. For sources of appreciable size the peak intensity is given first, followed by the integrated intensity in parentheses.

Next is given the relative spectral index, $(\alpha - \alpha_{M87})$, computed from the Cambridge and Caltech intensities. The final column lists the optical field class defined in Section V.

Remarks on individual sources follow. Sources that appear in other catalogues are indicated by MSH (Mills, Slee, and Hill[8]), W (Westerhout[11]) or HB (Hanbury Brown and Hazard[12]).

CTA 1: Faint wisp of emission on Schmidt plate agrees with radio-intensity distribution. Possibly supernova remnant.
NGC 281: H II region.
3C 32: MSH 01 − 12.
3C 33: Isolated elliptical galaxy.
3C 38: MSH 01 − 19.
3C 40: MSH 01 − 05. Pair of bright elliptical galaxies NGC 545/547.
3C 58: Spectral index, source size (preliminary Caltech interferometer result), and galactic latitude (+4°) indicate a galactic source.
3C 63: MSH 02 − 07.
3C 66: Elliptical galaxy that may have a jet (Minkowski, private communication).
3C 75: MSH 02 + 010. Pair of elliptical galaxies.
CTA 21: Rising background to north.
3C 89: MSH 03 − 03.
3C 98: Elliptical galaxy.
3C 123: W 7, IAU 04N3A.
Crab Nebula: Optical position given (calibrator).

Orion Nebula: Optical position given (calibrator).
S 147: Possible supernova remnant; source No. 74 of Gaze and Shaĭn.[13]
3C 161: MSH 06−04.
Rosette Nebula: Weak extensions to the north and east agreeing with optical emission.
3C 227: MSH 09+07.
3C 237: MSH 10+01.
3C 264: Preliminary interferometer observations indicate one source near the 3C position rather than the two sources that Elsmore observed.
3C 270: MSH 12+05. Elliptical galaxy NGC 4261.
3C 273: MSH 12+08, W 17.
M 87: Optical position given (calibrator).
3C 278: MSH 12−118. Pair of elliptical galaxies NGC 4782/4783.
3C 279: MSH 12−020.
NGC 5128: Centaurus A. Optical position given. Intensity based in part on Bolton and Clark.[14]
3C 298: MSH 14+05.
3C 310: Pair of elliptical galaxies.
3C 313: MSH 15+02.
3C 317: MSH 15+05.
3C 324: Confused by an extended source approximately 7^m later in right ascension.
3C 327: MSH 16+01.
3C 338: Multiple system of elliptical galaxies, NGC 6166.
3C 353: MSH 17−06, W 21.
MSH 17−16: May be two sources.
CTA 80: Source on intervening declination lobe between 3C 382 and 3C 384.
3C 392: MSH 18+011, W 44.
3C 398: W 49. Spectral index, source size (4′ Elsmore *et al.*[7]), and galactic latitude (−2°) indicate a galactic source.
3C 403: MSH 19+010.
Cygnus A: Optical position given (calibrator).
3C 424: MSH 20+010.
3C 433: Pair of galaxies.
CTA 97: Radio position just south of IC 5146, an H II region with a diffuse blue extension.
3C 444: MSH 22−17.
3C 445: MSH 22−09.
3C 459: MSH 23+05.
Cassiopeia A: Optical position given (calibrator).

Observations of Southern Sources

Description

In an effort to estimate the 960 Mc reliability of the survey of Mills, Slee and Hill (1958, 1960; hereafter referred to as "MSH"), a large fraction of sources listed in their catalogues down to an 85 Mc flux density limit of $15 \cdot 10^{-26}$ $Wm^{-2}(c/s)^{-1}$ have been observed by Kellermann and Harris (1960). A description of the observations and the results can be found in that report. Of interest to the present work, however, is the spectral information available from the intensity measurements.

The comparison of MSH-CT intensities differs in many respects from the 3C-CT work described in the last section. The circumstances which tend to enhance the accuracy of the MSH-CT comparison are threefold. First, the statistics are improved, since several hundred MSH sources contribute to the spectral index distribution rather than the ninety 3C sources listed in the CTA list. Another advantage of the MSH comparison is the longer frequency baseline afforded when computing spectral indices of MSH sources. Finally, the sensitivity of our receiver has been significantly improved over earlier observations and the collecting area has been doubled by using the interferometer.

On the other hand, the interferometer (18' lobe spacing) introduces a systematic error by resolving the larger sources.

A further systematic error will lower the 960 Mc intensity of sources if the position quoted by MSH is incorrect. This type of error would not, in most cases, affect the CTA list, which employed direction finding techniques. Finally, less time was spent observing each MSH source than was the case for the CTA sources. Thus, most intensity measurements of southern sources depend on a single observation of 3 to 6 interference lobes, while the intensities of northern sources are usually the averages of several observations on different dates. The details of these effects are given in the report of Kellermann and Harris.

Spectral Index Distribution

Hydra-A was observed as a calibrator each night, except when it crossed the meridian during the day. In the latter case, 3C 444 (MSH 22-17) was used as a secondary calibrator. By this method intensities were obtained as ratios to Hydra-A rather than as absolute flux densities. The results of the observations for 376 non-galactic sources which were not classified by MSH as "extended" or "possibly extended" are given in figure 3. In this type of presentation, we plot the log of the 960 Mc intensity ratio to Hydra-A as the ordinate while the abscissa is the log of the 85 Mc intensity ratio to Hydra-A. Thus the 45° line through Hydra-A will be the locus of points with relative spectral index equal to zero, while the relative spectral index for all other points is immediately apparent as proportional to the distance from the point to

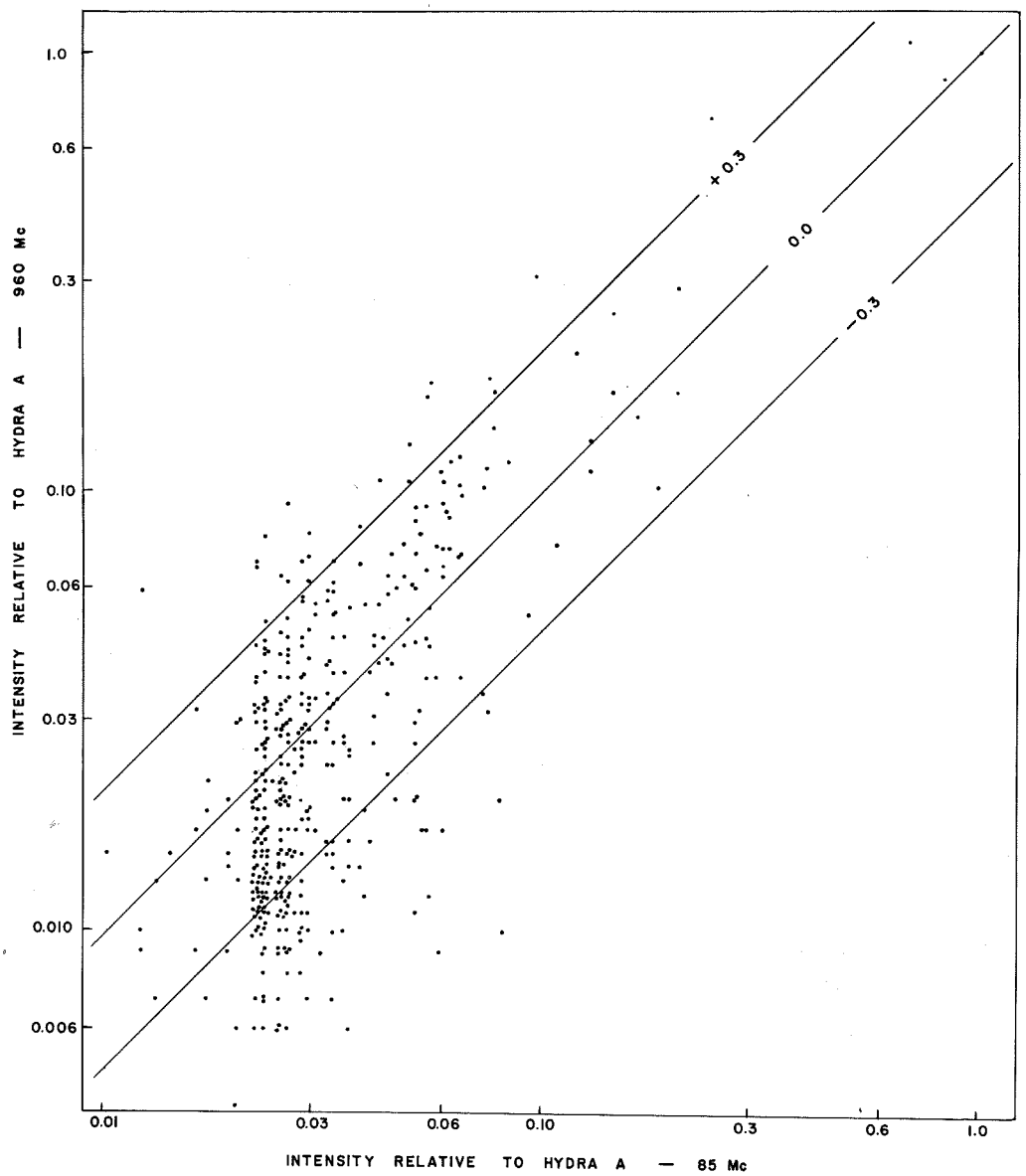

Figure 3 Two Frequency Intensity Comparison: 960 Mc - 85 Mc. Points for 376 "non-extended" sources with $b > 10^{\circ}$. Three 45° lines of constant spectral index are shown.

this line. Steeper spectra fall below the line and flatter spectra fall above it.

It is apparent from figure 3 that the average spectrum of the weakest source is somewhat steeper than that of the stronger sources. Although it might be tempting to ascribe this to some inherent characteristic of weak sources, it is more likely that this change of spectral index is due to increasingly larger position errors for weaker sources. Over the range of intensities of figure 3, the mean spectral index shifts from about +0.10 to -0.10: i.e., an intensity change of 1.0 to 0.6. If this were to be accounted for entirely by inaccuracy in the quoted 85 Mc positions, our antennas would have to be aimed, on the average, about 20' off the source for the weakest objects. Alternatively, if the interferometer were resolving some of the sources, this would tend to have a similar steepening effect on the spectra. Resolution at the 200-foot spacing will reduce a 5' diameter gaussian source to 75% and a 10' source to 33% of its true intensity. However, one would not expect the effects of resolution to increase for the weaker (presumably smaller) sources.

Comparison with the Northern Sources

The median spectral index for all the MSH sources considered here is -0.07 and 75% of the sources lie within 0.3 of this median (i.e. between a relative spectral index of -0.38 and +0.22). This characteristic spread of ±0.3 in the spectral index distribution is not significantly different

from that observed in the Cambridge-Caltech comparison (±0.25). Figure 4 presents the 3C-CT data for comparison with figure 3.

The relation of the median spectral index of the two distributions depends on a reliable spectrum of Hydra-A relative to M87. From the CTA list, the spectral index of Hydra-A is +0.09 relative to M87 (which gives $x_{Hydra-A}=-0.63$ if $x_{M87}=-0.72$). A direct comparison of the flux density at 85 Mc and 960 Mc yields $x_{Hydra-A}=-0.96$. Goldstein (1960) quotes a value of -1.02 when he compares his 1420 Mc Harvard observations with the MSH intensity of Hydra-A. Whitfield (1957) quotes -1.0. In view of these discrepancies, we have plotted in figure 5 observations of Hydra-A at several frequencies where ratios to M87 are available. From figure 5 the spectral index relative to M87 is 0.0 ± 0.1. Thus, if $x_{Hydra-A}=x_{M87}$ the median value of the spectral index distribution for the more intense MSH sources agrees with the median value of the 3C sources. This is consistent with the interpretation of position errors tending to produce apparently steeper spectra for the weaker sources. The interferometer observations have thus extended our knowledge of the spectral index distribution to many more sources than contributed to the CTA list.

Remarks

Under the assumptions of synchrotron emission and an exponential energy distribution of the relativistic particles

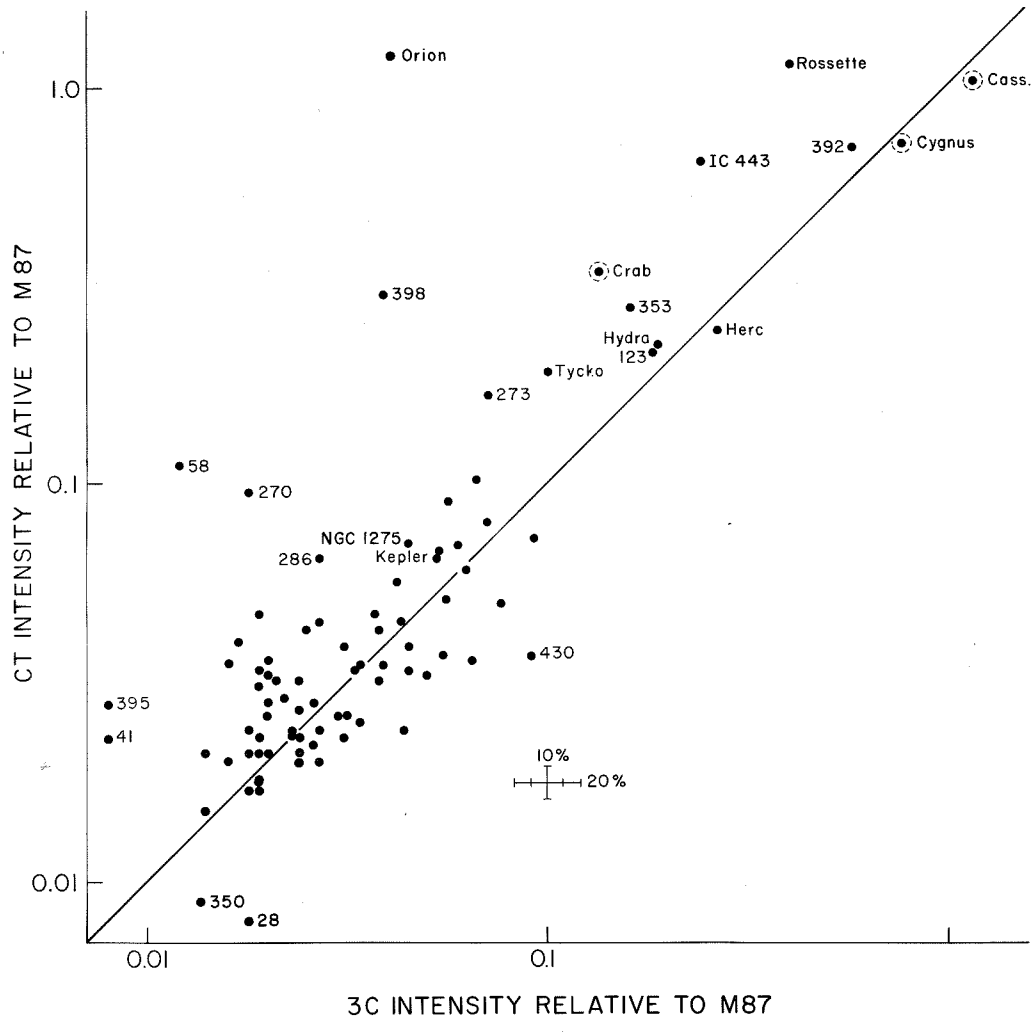

Figure 4 Two Frequency Intensity Comparison: 960 Mc - 159 Mc. Numbers refer to the 3C source name.

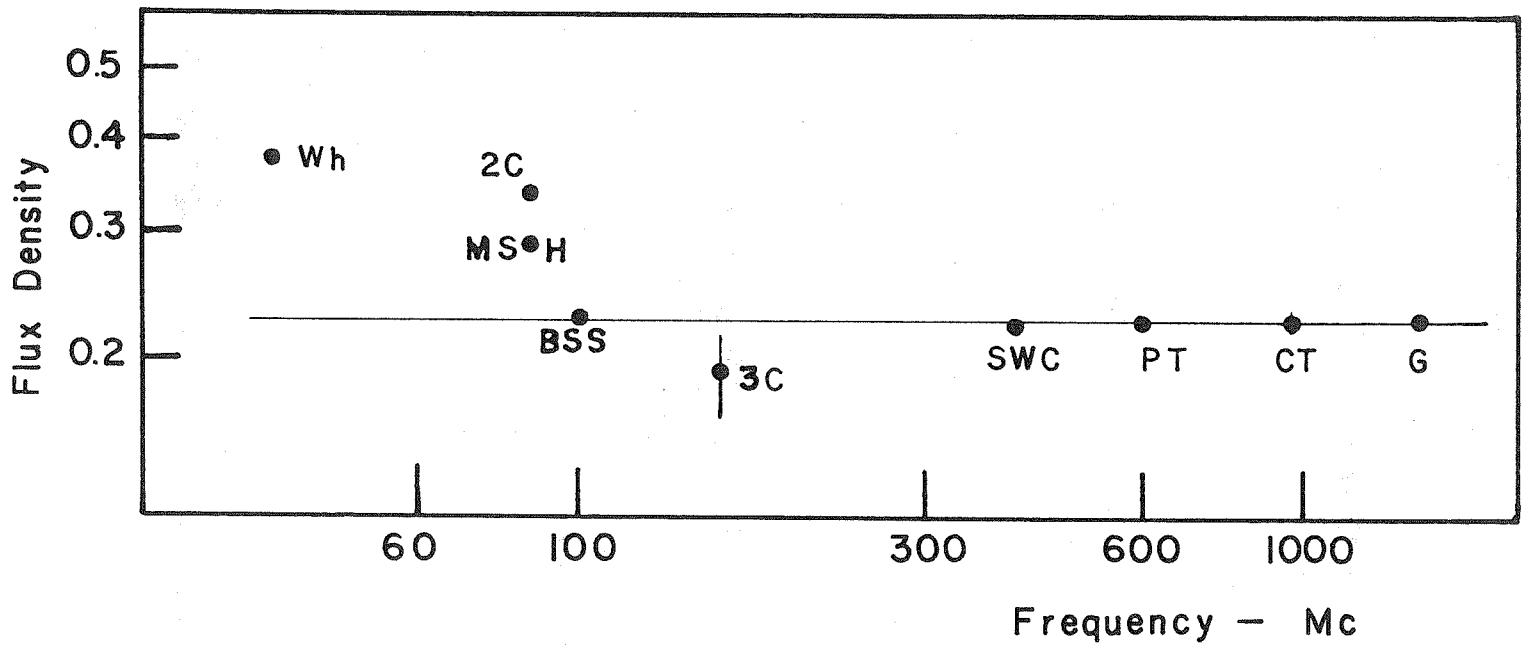

Figure 5 Spectrum of Hydra A Relative to M87.

Wh - Whitfield, 1957
2C - Shakeshaft et al, 1955
MSH- Mills, Slee, & Hill, 1958
Mills and Slee, 1957
BSS- Bolton, Stanley, & Slee, 1954
3C - Edge et al, 1959
SWC- Seeger et al, 1957
Seeger et al, 1956
PT - Piddington and Trent, 1956
CT - Caltech, present observations
G - Goldstein, 1960

responsible for the observed radiation, the exponent of this distribution can be found from the observed spectral index. This procedure will be described in Part II, but it is interesting to note that the median spectral index of -0.65 ± 0.10 found above corresponds to a particle distribution of the form, $N=\text{const. } E^{-2.3\pm0.2}$ (where E is the energy of the particle and N is the number of particles with energy between E and E+dE). The value of the exponent, -2.3, is close to that of the cosmic ray distribution, -1.9 to -2.2 (Ginzburg, 1958). Implications of this similarity have been discussed by authors such as Gold and Hoyle (1959), and Ginzburg (1959), and may eventually lead to an understanding of the high luminosity radio galaxies and their relation to normal galaxies such as our own. If the same process is responsible for the emission of most external sources, the variations in energy distributions of the relativistic electrons may reflect different stages, or differences of initial conditions, of any such process.

Part II - Supernova Remnants

A. Introduction

This part of the thesis investigates the radio emission of 13 non-thermal galactic sources and attempts to find relationships among them. Although only 3 of these radio sources are known to be the remains of supernova outbursts, the rest are generally considered to be supernova remnants also. Several of them show expansion (e.g. the Cygnus Loop and Cas-A) and almost all of them show some indication of shell structure.

With the exception of the galactic spur (Hanbury Brown et al, 1960), all proposed supernova remnants known to us are listed in Table II. The fact that a relation between the age and spectral index of 13 of these objects can be found (Part II, Section E) enhances the probability that most of these 13 sources do belong to the same group of physical objects.

The smaller supernova remnants have been studied previously by many workers and do not lend themselves to extensive investigation with the present equipment. Therefore, most of the observational effort has been spent on the larger objects. The Cygnus Loop is a stronger source than most other similar remnants, and has been observed in more detail. Therefore, it is presented here as a proto-type of the larger objects and the first section treats the spectrum and emission process of this source. Arguments are given to show that the

Table II - Proposed Supernova Remnants

Object	I_{960}	α (1950)	δ	
A) Objects studied in the present paper.				
Cas A	3120±150	$23^h21^m11^s$	$+58^o32'$	Expanding Shell
Pup A	132± 12	08 21 20	-45 52	Similar to Cas A
Kep. SN	22± 3	17 27 40	-21 25	S.N. observed
Tyc. SN	57± 3	00 22 46	+63 51	S.N. observed
W 44	211± 9	18 53 35	+01 15	Shell; NT.spec.
IC443	195± 24	06 14 16	+22 36	Similar to C.L.
Crab N.	1030± 45	05 31 30	+21 59	S.N. observed
HB21	180± 60	20 44 42	+50 32	
Cyg. L.	265± 50	20 50	+30 30	Expanding Shell
Vela X	1400*	08 32 48	-45 37	Similar to S147
HB9	160± 30	04 57 30	+46 25	
S147	120± 60	05 36	+28	
CTA 1	75± 18	00 02 35	+72 04	Emission Arc
B) Other Radio Sources of similar type.				
NGC6888		20 10 55	+38 15	Similar to C.L.
CTB1	56*	00 00 18	+62 11	Faint ring
CTB13	225*	04 24	+47 00	
W28	240*	17 58 12	-23 22	N.T. Spectrum
Shklovsky's Selection of extended galactic objects.				
HB 3		02 16	+62 30	(1960b)
HB 7		03 23 30	+55 06	
HB 8		04 02	+47 30	
Vela Y	120*	08 43	-43 31	
Vela Z	40*	08 45 42	-45 03	
Cent.B		13 22 48	-59 24	
C) Optical Objects:				
Minkowski's small objects (1958)				
		07 12	-13	Peculiar Double Ring
S22		01 27 28	+58 06	
		07 26 15	+13 21	
Van den Bergh's Filaments (1960)				
No. 2		05 24	+42 56	Low Density Ring
No. 6		18 02	-23 40	

* Indicates CTB Flux Density used. (Wilson and Bolton 1960)

I_{960} is the Flux Density at 960 Mc/s measured in units of 10^{-26} watts $m^{-2}(c/s)^{-1}$.

radio emission of the Cygnus Loop is not primarily due to free-free transitions in the ionized hydrogen filaments, and even though the emission is probably of a non-thermal character, the spectrum is considerably flatter than the average non-thermal spectrum.

Next, the other remnants are examined, and the following two sections give the spectrum and space distribution of the emission. The spectral indices for the 13 sources studied range from -0.8 to +0.5, although the positive values are doubtful due to large errors. Extrapolating these spectra to optical frequencies suggests that except for the Crab Nebula, non-thermal emission would not necessarily be observable on the Sky Survey plates of the 48" Schmidt. Even though the optical emission is probably not due to the same mechanism as the radio emission, the spatial coincidence must be explained and this is considered briefly.

Finally, the time variation of the spectral index is examined by correlating increasing diameters and decreasing surface brightness with advancing age. This leads to the conclusion that the spectrum flattens with age. Such a process requires changes in the energy distribution of the relativistic particles responsible for the radiation (assuming synchrotron radiation), and the last section considers this problem.

B. Cygnus Loop Detail

Intensity Measurements

The present observations of the Cygnus Loop consist of

about 30 drift curves of 40 minutes each taken at one-half degree intervals between +27°30' and +33°30'. These intensity records, obtained between April and November 1959, were normalized by a drift curve at δ=30°00' taken each night. Figure 14, Appendix IV, shows the resulting Cygnus Loop contours of antenna temperature where a linear subtraction for the galactic background has been made. The galactic correction was performed on the average drift curves by noting the slope of the antenna temperature as the galaxy left the antenna beam before the source was encountered. The background was usually less than 20% of the source's peak intensity by the time the western peak was reached.

Following Mathewson, Large and Haslam (1961), hereafter referred to as "MLH", the Loop was divided into three parts: A, B, and C. The strongest part, A, is in the southwest; B is in the northwest; and C is in the northeast section, coinciding with NGC 6992-5. Each part was integrated with a planimeter, thus giving an integrated value of intensity for the individual sections as well as for the complete source. The intensity of the total source published by Harris and Roberts was based on a preliminary contour diagram and the value given here supercedes that.

The contour map may be considered as a representation of a 3-dimensional model of the radio energy received from the sky. In such a model, the antenna temperature determines the altitude of any point (α,δ), above the reference plane

(T_a=0°K). The integrated flux density from any source is proportional to the volume under the continuous surface of antenna temperature. It is then possible to define a quantity which measures the extent to which a source broadens the antenna beam:

$$B=\frac{\int T_a \, d\Omega \text{ (source)}}{R \cdot \int T_a \, d\Omega \text{ (Reference Source)}}$$

where R is the ratio of the peak intensity of the source to that of the reference source. The orginal contour map integration (used in the CTA list), gave B=7.54. The final contour map (figure 14) includes more observations and gives B=8.95. The 'best value' is taken as B=8.5±1.0.

The value of R (relative to M87) was determined from the average of 7 drift curves taken at δ=+30°00'. Combining this R=0.104±0.008 with B=8.5±1.0 yields a total integrated intensity for the Cygnus Loop of 0.88±0.17.

Several observations have been made at other frequencies. These are presented in Table III. For the purpose of deriving a spectral index, it is valuable to obtain intensities as ratios to standard sources, rather than relying on published flux densities. The results of this approach will yield the spectrum of the Cygnus Loop relative to that of the standard source (in this case, M87). This was the method used in Part I for the spectrum of Hydra-A (figure 5). However, the data for the Cygnus Loop at other frequencies is not uniform

Table III - Cygnus Loop Flux Densities.

Frequency Mc	Flux Density $Wm^{-2}(c/s)^{-1}$	Beamwidth degrees	Observer
38	750 ± 200	0.6 x 40.	Costain †
81.5	470 ± 150	2. x 15.	Baldwin, 1955
92.5	220*± 100	3.	Walsh & Brown, 1955
158.	350*± 70	1.6 x 2.2	Mathewson, Large and Haslam, 1961
178.	430 ± 80	0.2 x 4.6	Baldwin & Leslie, 1960
400.	268*± 50?	2.1	Westerhout, 1960
408.	260*± 50	0.7 x 0.9	MLH, 1961
915.	100*± 25	1.7	Eaton & Kraus, 1959
960.	265*± 50	0.8	Caltech
1390.	80*± 20	0.57	Westerhout, 1958

* Normalized by intensity ratios to strong sources. See text.

† Reported by Baldwin and Leslie (1960)

(i.e. ratios to M87 are not always available). In order to consider all the information, we have normalized quoted flux densities to a given spectrum of M87 wherever possible, and otherwise used flux densities as quoted. So long as the dependence of the derived spectrum on that of the reference source is realized, this method is equivalent to plotting ratios with respect to the standard source (as in figure 5). Thus the normalizing procedure should not be viewed as a correction of published flux densities; rather it is an attempt to relate all observations to some arbitrary reference spectrum.

Two other sources were used as secondary calibrators. Cas-A was the source used to normalize Westerhout's 400 Mc value and 3C 295 was used as a standard by MLH at 158 Mc and 408 Mc. The relevant spectra adopted are as follows:

$S_{M87} = 42{,}000\ f^{-0.72}$ CTA

$S_{Cas\text{-}A} = 757{,}000\ f^{-0.8}$ Whitfield, 1957

$S_{295} = 948\ f^{-0.5}$ CTA

where S is in units of 10^{-26} $Wm^{-2}(c/s)^{-1}$ and f is in Mc. These spectra are mutually self consistent. (Whitfield's spectrum of Cas-A gives $S_{960}(Cas\text{-}A) = 3110$ - cf. CTA value of 3120 - and the CTA spectrum of 3C 295 gives the same values quoted by MLH at 408 Mc and 158 Mc.) Therefore, the spectrum derived for the Cygnus Loop will reflect any errors in the spectrum of M87, but should not be very sensitive to the values used for the other sources.

Spectrum of the Cygnus Loop

The results of Table III are plotted in figure 6. The interpretation in terms of spectral index must rest on a subjective choice of which data to weight most heavily. Mathewson, Large and Haslam have suggested that Westerhout's flux density of the Cygnus Loop at 1390 Mc may be low because of failure to detect the weaker sections of the source. The same comment may be made of the 915 Mc value of Eaton and Kraus. In addition, however, there is some doubt of the reliability which should be ascribed to the 915 Mc source list. HB21 was not detected by Eaton and Kraus even though the CTA peak intensity of this source is twice as great as that of the Cygnus Loop. Also, Moffet (1960) was unable to verify 18 of the 24 sources listed by Eaton and Kraus.

Costain's measurement at 38 Mc employed a corner reflector with a 40° beam to half power points in declination. As HB21 is only 20° away, and the galaxy is even closer, we feel his intensity error should be increased by an unknown factor.

The line drawn in figure 6 has a slope of -0.10. If the spectrum does follow a simple power law as assumed, the spectral index is $x_{CL} = -0.10 \pm 0.10$. The error quoted for this value was estimated by fitting lines of various slopes to the data of figure 6. It is felt that the probability of the spectral index lying between 0.0 and -0.2 is about 60%. In this case the error is chiefly determined by the lack of agreement of the low frequency intensities rather than by the

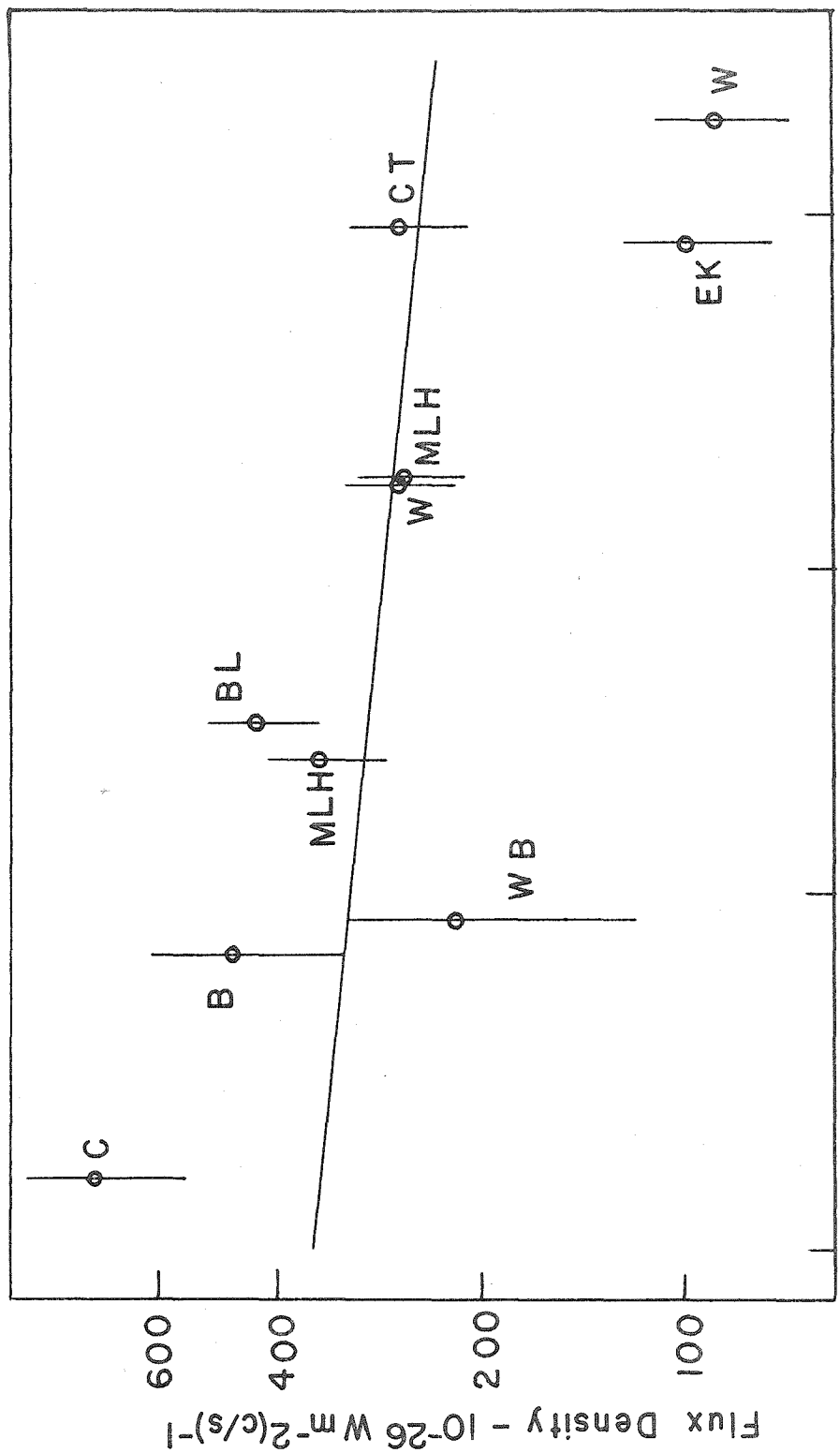

Figure 6 Spectrum of the Cygnus Loop. The individual values are given in Table III.

errors quoted for the individual measurements.

Mathewson, Large and Haslam divide their contour map into three sources and compare brightness temperatures at 158 Mc and 408 Mc in order to derive spectral indices of the separate components. Unfortunately, at 158 Mc their beamwidth is significantly different than at 408 Mc, and they are forced to artificially widen their 408 Mc beam to an equivalent $1\overset{\circ}{.}6 \times 2\overset{\circ}{.}2$.

Fortuitously, our 960 Mc beamwidth is almost identical to that of MLH at 408 Mc. Therefore, it is possible to derive a spectral index for each part of the Loop by integrating the three sources separately. The contour map was divided by 'paths of steepest descent' (dotted lines on figure 14). The 408 Mc map was then integrated over the same boundaries and all three parts were found to contribute essentially the same percentage of the total emission as they did at 960 Mc. This conclusion is confirmed for Source C by the estimate of Baldwin and Leslie (1960) that 40 of the total 430 $\left[10^{-26}\ \mathrm{Wm^{-2}(c/s)^{-1}}\right]$ at 178 Mc could be attributed to the eastern hump in their contours; i.e., NGC 6992-5, or Source C. This agrees very well with the fractions obtained at 408 Mc and 960 Mc, although the absence of a secondary peak (Source C) on Costain's 38 Mc record led Baldwin and Leslie to conclude that the spectral index varied across the Loop.

Table IV lists the pertinent data. First it compares the 960 Mc positions with the 408 Mc positions for reference.

Table IV - Spectral Index of the 3 parts of the Cygnus Loop

Item	Frequency	A	B	C
α (1950)	960	$20^h48^m.4 \pm 0.3$	$20^h46^m.6$	$20^h53^m.3$
	408	$20\ 48.3 \pm 0.3$	20 46.7	20 53.3
δ (1950)	960	$+29^\circ52' \pm 5'$	$+31^\circ27'$	$+31^\circ37'$
	408	$+29\ 40 \pm 5$	+31 28	+31 28
Integrated Intensity (percent of total)	960	64%	25.8%	10.2%
	408	62%	28%	9.7%
	178			9.3%
Spectral Index, relative to that for entire Loop	960-408	+0.03	-0.09	+0.06
	960-178			+0.05

Then the results of the integrations are given. From these values, spectral indices of A, B, and C are computed relative to the spectral index of the entire Loop.

The Process Responsible for the Radio Emission

Free-Free Transitions. In Part I it was shown that most radio sources have spectral indices of -0.65 ± 0.25. The notable exceptions to this rule are the galactic sources which may have flatter spectra with indices in the neighborhood of zero. As this is the value of spectral index expected for optically thin H II regions, it is often the case that the occurrence of a nearly flat spectrum is classified "thermal" with the implication that free-free transitions in ionized hydrogen are the source of the radiation (e.g. Wilson and Bolton, 1960).

This line of reasoning has been extended to the Cygnus Loop by Mathewson, Large and Haslam (1961), who treat the spectrum of Source C as the combination of a "thermal" component with $x = 0$ and a "non-thermal" component with $x = -0.5$. This interpretation was encouraged by the observation of MLH that the spectral index of the optically bright region, Source C, was flatter than that of the brightest radio region, Source A. However, in the light of the results of figure 6 and the integrations summarized in Table IV, it seems advisable to reconsider assumptions which disregard the occurrence of flat, non-thermal emission.

From an order of magnitude count of filaments throughout

the Cygnus Loop, it appears that Source A should have about one-half as much thermal emission as Source C. However, the integrations of Table IV show that A contributes over six times more radio emission than does C. Therefore, even if Source C were entirely thermal, Source A would be 90% non-thermal. Furthermore, it is quite obvious from figure 7 that the radio emission of Source A is centered well away from the main group of filaments. These considerations demonstrate that a fairly flat spectrum does not necessarily imply the existence of free-free emission.

Although Source A is due to non-thermal mechanisms, the emission from Source C is generally considered to be a combination of thermal and non-thermal radiation (Baldwin and Leslie, 1960; MLH, 1961). To derive an independent estimate of the importance of the free-free process in Source C, we have used optical measurements to calculate the expected radio emission (Appendix I). These calculations are based on Chamberlain's observations (1953b) of the surface brightness in Hα of several filaments in the Cygnus Loop. It has been assumed that absorption of the Hα intensity by interstellar dust is negligible. This is verified by star counts which were made in selected regions extending from the Loop toward the galactic plane (Bok and Warwick, 1957). Although blue plates revealed 1 to 4 magnitudes of absorption at 500 or 1000 pc, the red (λ6300) absorption was generally small, and in the immediate vicinity of the Loop, it was less than one-half magnitude.

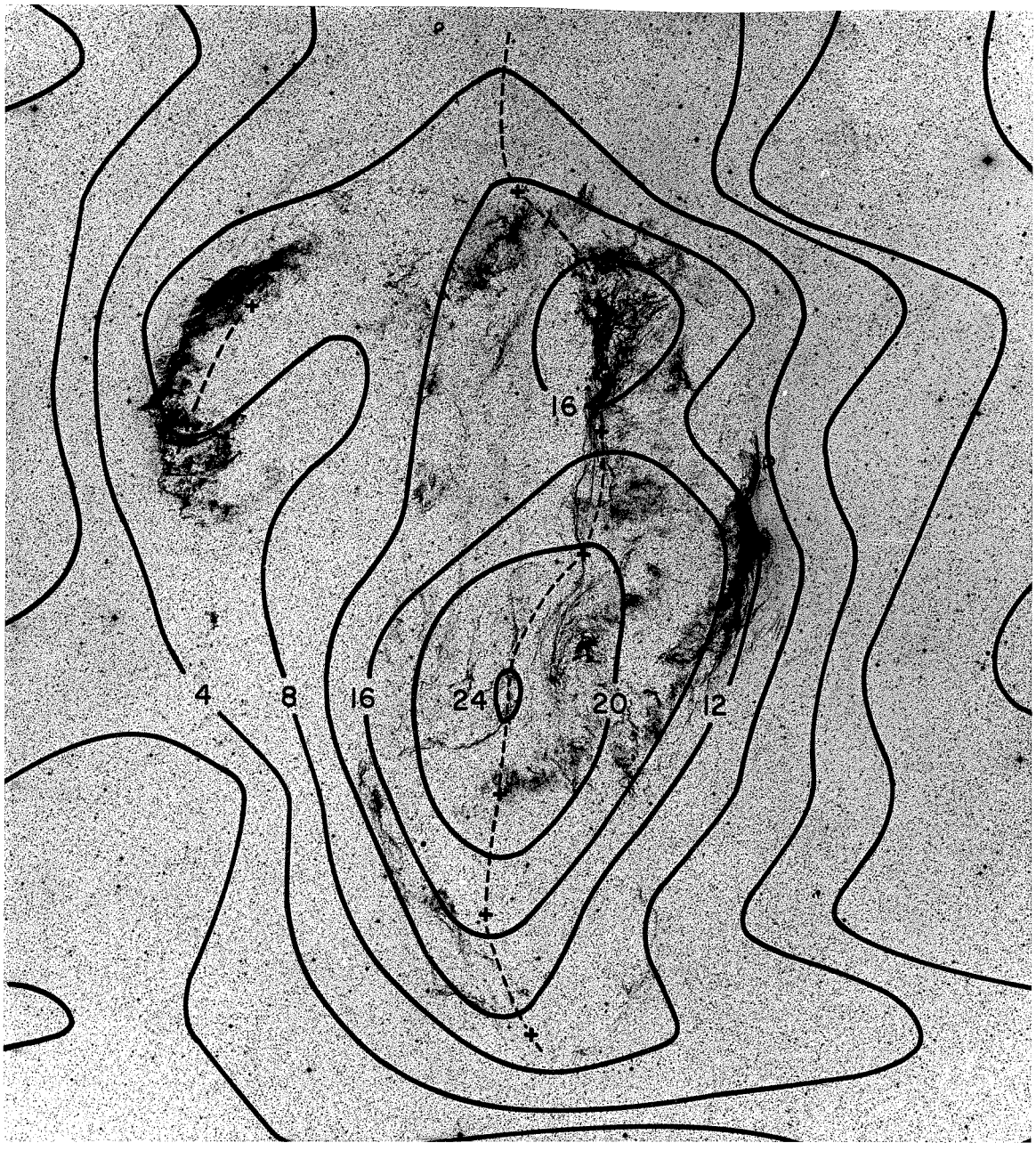

Figure 7 Comparison of the Radio and Optical Emission from the Cygnus Loop. Contours of antenna temperature (arbitrary scale) are the same as in figure 14.

The chief source of error in the calculation of expected radio emission is due to the uncertainty of the estimated area which is appropriate for the surface intensity measurements of Chamberlain. We have taken the area as 250 filaments of size quoted by Osterbrock (1958): $1\overset{''}{.}8 \times 4\overset{'}{.}5$. This figure may contain an error of a factor of two. The calculations predict that 4% of the total radio emission from Source C is contributed by free-free transitions in the filaments. An additional 2% may come from a hypothetical sheet of ionized hydrogen which is undetected by even the deep red plates of the 48" Schmidt. Although the calculated free-free radiation is small (4 to 6%), it is not possible to rule out a significant contribution to the radio emission of Source C by this process.

Appendix I also contains estimates of the free-free emission from HB9, where it has been assumed that the light is due to Hα emission. We have used the "plate limit" calculation of Appendix I, as HB9 is barely visible on the E plate of the survey, but is quite evident on Minkowski's deep red plates (figure 19, Appendix IV). The calculations give an expected free-free emission = 2.5% of the total radio emission from HB9. The most uncertain quantity in this calculation is the interstellar absorption, which has again been neglected because there are a few galaxies visible in the field. If two magnitudes of absorption were present, it would raise the computed 2.5% to 16%.

A similar figure holds for HB21 which is even fainter optically and slightly brighter at 960 Mc than HB9. Furthermore, comparatively strong emission (presumably Hα) to the southwest of HB21 produces barely detectable radio flux (compare figures 16 and 20, Appendix IV). Therefore, with the possible exception of Source C of the Cygnus Loop, thermal emission may be discounted as seriously influencing the observed radio emission.

Synchrotron Emission and Polarization of the Cygnus Loop. If the radiation from the Cygnus Loop is due to the synchrotron process, the most obvious experiment is to search for linear polarization. Besides the sun, polarization in the radio region has been detected only from the Crab Nebula (Mayer et al, 1957), M87 (Barat et al, 1960), and Jupiter (Radhakrishnan and Roberts, 1960). Furthermore, although the Crab Nebula is known to be strongly polarized in the optical continuum, the amount of polarization at 3 cm is only a few percent, and at 20 cm it appears to be less than 1% (Westerhout, 1956).

It is possible that the Cygnus Loop may contain a large scale magnetic field, since the filaments are ordered over dimensions comparable with the size of the Loop. Thus, even though polarization has been difficult to observe in many small sources, it was hoped that the conditions might be more favorable in the Cygnus Loop. Observations were taken during November 1959, to see if a measurable fraction of the radia-

tion was linearly polarized. The equipment was identical to that used for the other observations reported in this paper. Appendix II describes the procedure and results.

Although the observations are consistent with a radial magnetic field producing about 15% polarization, the techniques used were not accurate enough to provide a positive detection of a polarized component of the radio emission. Thus, the exact nature of the emission process in the Cygnus Loop remains unknown, although the predominant contribution must be non-thermal in character.

C. Frequency Dependence of the Radio Emission

Spectral Indices

With the Cygnus Loop as a proto-type, it is now pertinent to consider the other supernova remnants. Once again, we begin the study with a determination of the spectra of these objects.

The spectral indices listed in Table X (Appendix III) are based on the values of the CTA list unless supplementary information would change the spectral index significantly. For the Crab Nebula, a value of -0.25 is adopted. This is an average between the CTA value of -0.21 and the Dutch value (Woltjer, 1958) of about -0.3. Flux densities for sources which have been examined in more detail are listed in Table V and plotted in figure 8.

The spectra of S147 and CTA1 are not well determined since they depend on only two points of low accuracy (960 and

Table V Supernova Remnants - Flux Densities.

Source	Spectral Index	1420 Mc	960 Mc	600 Mc
Puppis A	-0.66±0.20		132±12	
Kepler's SN	-0.54±0.10		22* 2	
IC 443	-0.37±0.10	188± 8 Wa (215)	195±24	256 PT
		121 HLM (160)		
HB 21	-0.17±0.20		180±60	
Vela X	-0.05±0.15		1400 CTB	
HB 9	+0.20±0.20		160±30	
S147	+0.45±0.8		120±60	
CTA 1	+0.56±0.6		75±20	

* CTA value corrected for pointing error in the CTA list.

Parentheses indicate published flux densities, while the rest of the values have been normalized to our spectrum of M87: $300 \cdot 10^{-26} \mathrm{Wm}^{-2}(\mathrm{c/s})^{-1} = (\mathrm{const}) \cdot (960)^{-0.72}$

CTB -Wilson and Bolton (1960)

HMS -Haddock, Mayer and Sloanaker (1954)

MS -Mills and Slee (1957)

MSS -McGee, Slee, and Stanley (1955)

MSH -Mills, Slee, and Hill (1960)

PT -Piddington and Trent (1956)

Ra -Rishbeth (1956)

Rb -Rishbeth (1958)

Table V (Continued)

Source	400 Mc	159 Mc	86 Mc	19 Mc
Puppis A	(250) MSS		(690±100) S	(800) Rb
Kepler's SN		58±12 3C	77 MSH (110)	
IC443	305 SWvH (250)	270±40 3C	485** Ra (660)	
HB 21	173±60 Wb	280±70 BH (200)		
Vela X			(1600) Rb	(360) Rb
HB 9	132±25 Wb	112±28 BH (80)		
S147	81±40 Wb			
CTA 1	46±20 Wb			

**Normalized to M87 by use of MS value of M87 and the Crab Nebula.

BH -Brown and Hazard (1953)

HLM -Hagen, Lilley, and McClain (1955)

SWvH-Seeger, Westerhout, and van de Hulst (1956)

S -Sheridan (1958)

Wa -Westerhout (1958)

Wb -Westerhout (1960)

3C -Edge, etal. (1959)

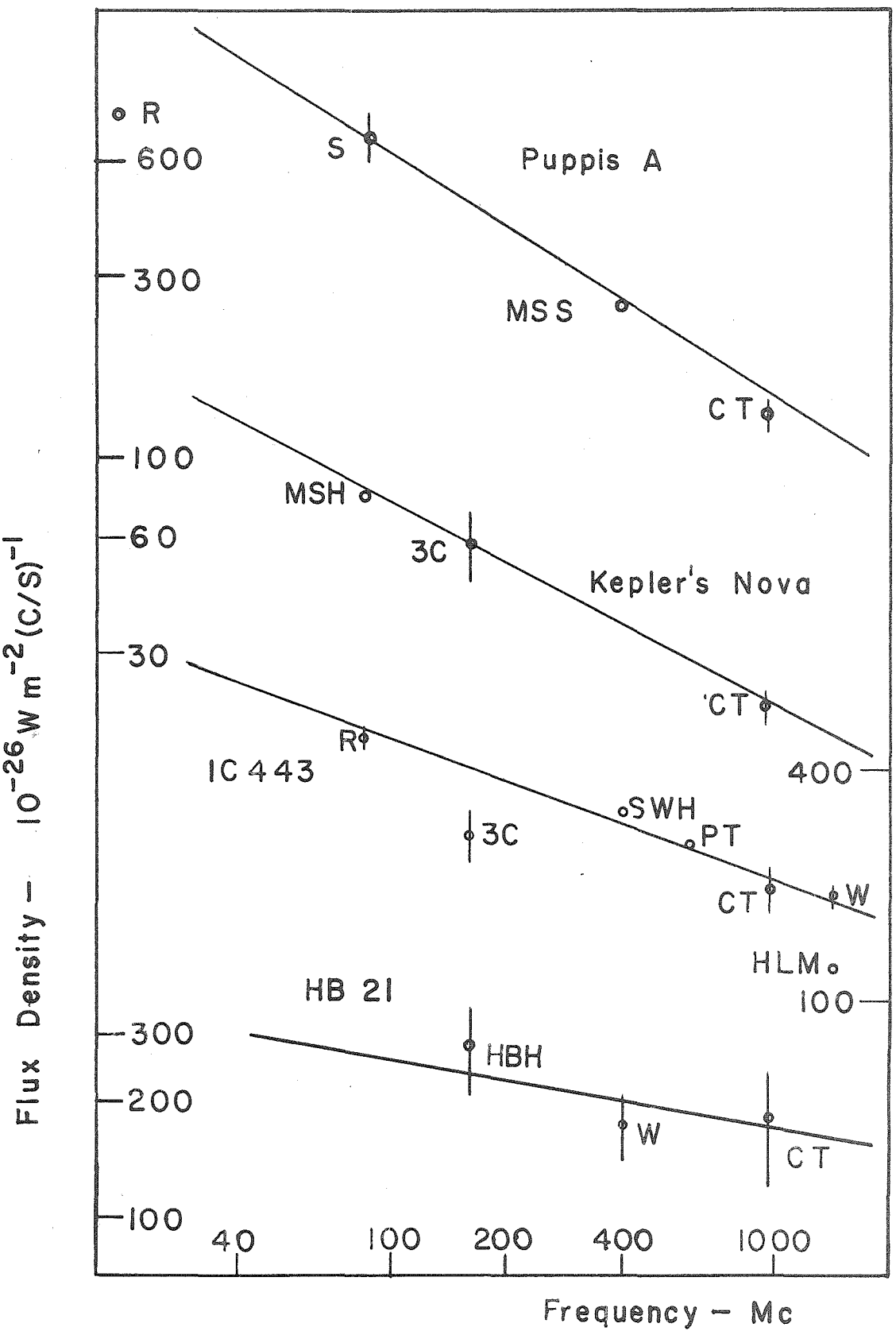

Figure 8 Spectrum of Supernova Remnants.
See Table V for the values of flux density.

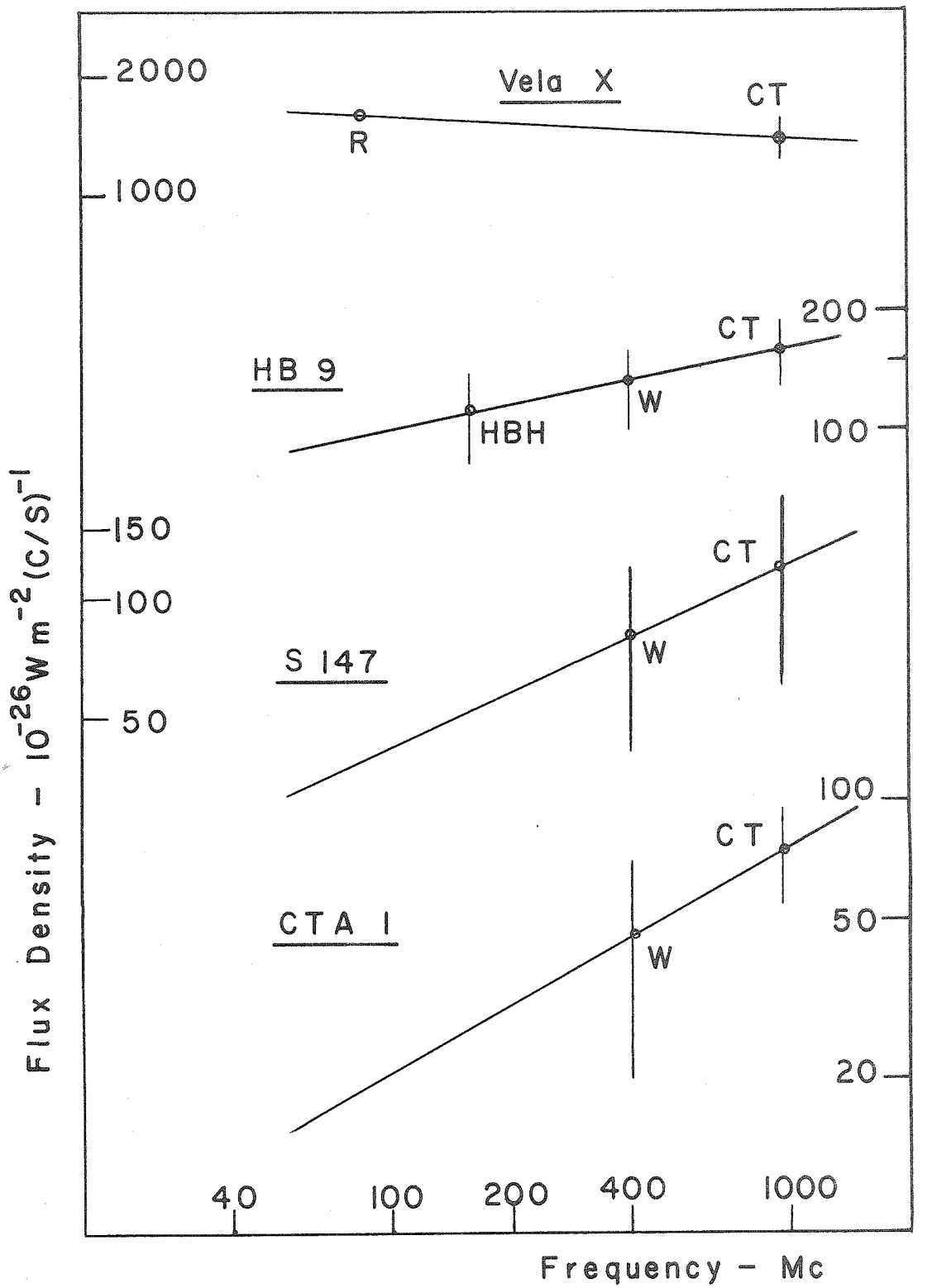

Figure 8 (Con't) Spectrum of Supernova Remnants.
See Table V for the values of flux density.

400 Mc). As in the case of the Cygnus Loop, the 400 Mc intensities of Westerhout were changed slightly in order to achieve a spectrum relative to that of M87:
$300 \cdot 10^{-26}$ $Wm^{-2}(c/s)^{-1} = A(960)^{-0.72}$.

For HB9 and HB21 flux densities are also available at 159 Mc (Hanbury Brown and Hazard, 1953). An attempt to normalize the Brown and Hazard values to the 3C intensity scale was made by computing intensity ratios for the ten sources common to both lists. $S_{3C}/S_{B\&H}$ varied from 0.32 to 1.85 with Cas-A = 1.4 and Cyg-A = 1.5. The average of all ten values is 1.2. A normalization factor of 1.4 is adopted.

The slopes of the straight lines of figure 8 are listed in Table V. These spectral indices are the ones used in all further calculations and correlations. The errors quoted for the spectral indices are estimated by fitting lines of different slopes to the plotted flux densities. These errors are more apt to depend on the quoted flux density errors than was the case for the Cygnus Loop spectrum.

The Possible Existence of a High Frequency Cutoff to the Non-Thermal Radio Spectrum

With the exception of the Crab Nebula and M87, our knowledge of non-thermal emission from radio sources is limited to frequencies below 10,000 Mc. This absence of information has led to the practice of assuming that the radio spectrum falls to zero at some cutoff frequency (e.g. Burbidge and Burbidge, 1959). Minkowski has suggested that it might be

possible to demonstrate the reality of such a cutoff by extrapolating the radio spectrum to optical frequencies. If an observable continuum is predicted by this extrapolation while only emission lines are present, then a change in the spectral law, such as the proposed cutoff, would be required. This section presents calculations of optical surface brightness for several supernova remnants, for the sky background, and for the limit of detection on survey plates.

According to Allen (1955), the night sky has a surface brightness approximately equal to 300 10th magnitude stars per square degree. This is equivalent to 23 stars of the 25th magnitude per square second of arc. The limit of detection, however, is much fainter than the sky background. Abell quotes a figure of 26 or 27 magnitudes per square second of arc for the limit of visibility on the O plates of the sky survey (Abell, 1960).

In order to compare surface brightness in magnitudes per square second of arc with that expressed in $Wm^{-2}(c/s)^{-1}$ (min. of arc)$^{-2}$, we use Woltjer's measurement of the Crab Nebula (1958). The integrated visual magnitude of the continuous radiation from the Crab Nebula is 8.64. If the area is taken as 4.8 square minutes of arc, a surface brightness of 19.2 magnitudes per square second of arc is obtained. This is equivalent to 200 stars of the 25th magnitude per square second of arc, i.e. about 8.7 times the sky background.

Table VI gives the expected optical emission of selected remnants assuming that the radio spectrum is extrapolated to

Table VI - Optical Extrapolation of the Radio Emission for Selected Supernova Remnants.

Source	Spectral Index	Area (sq. min.)	Surface Intensity at 10^{15} c/s			
			$Wm^{-2}(c/s)^{-1}(sq.')^{-1}$	Rel. to Crab	Rel to Sky	Rel to Pl. Lim.
Cas A	-0.77	12.5	$6.54 \cdot 10^{-29}$	0.00098	0.0085	0.49
Kepler's S. N.	-0.54	< 3.1	$2.0 \cdot 10^{-29}$	0.00030	0.0026	0.15
Tycho's S. N.	-0.53	28.	$1.3 \cdot 10^{-29}$	0.00019	0.0016	0.09
Crab Neb.	-0.25	4.7	$6.66 \cdot 10^{-26}$		8.7	500.
Cyg. Loop	-0.10	25,400.	$2.62 \cdot 10^{-29}$	0.00039	0.0034	0.19
Vela X	-0.05	14,100.	$5.0 \cdot 10^{-28}$	0.0075	0.065	3.8
HB 9	+0.20	16,300.	$1.6 \cdot 10^{-27}$	0.024	0.021	12.

10^{15} c/s. The last four columns list the surface intensity in $Wm^{-2}(c/s)^{-1}(min.\ of\ arc)^{-2}$; the surface intensity relative to that of the Crab Nebula; the surface intensity relative to the sky background; and the surface intensity relative to that which would be at the limit of detection (26 magnitudes per square second of arc).

On the basis of these calculations, one would not expect to observe any optical radiation from the Cygnus Loop or from most of the other sources. Although the extrapolated emission of HB9 is a factor of 12 above the plate limit, the uncertainty in the spectral index allows a flux density at 10^{15} c/s, 1000 times less than that listed in Table VI. Therefore the present calculations do not necessitate any departure from the radiation spectrum determined by radio observations.

A further extrapolation which extends well beyond the Lyman limit would enable an estimate to be made of the energy available for hydrogen ionization. This calculation was suggested by Münch on the basis of the work by Oort and Walraven on the Crab Nebula (1956). The later authors found that there was ample energy beyond the Lyman limit to ionize the hydrogen of the filaments. The difficulties of applying a similar explanation to the Cygnus Loop are that the optical emission, if present, is not measurable and therefore the extrapolation must be predicted from the radio frequencies. Secondly, the Balmer decrement in the Cygnus Loop has been interpreted by Minkowski (1958) to favor collisional excita-

tion. However, these measurements do not forbid radiative excitation, and therefore we make the following order of magnitude energy calculation.

If the extrapolated radio spectrum is integrated between λ100 and λ915, the power available to ionize hydrogen will be given by:

$$P = 4\pi R^2 \int_{3.3\cdot10^{15}}^{3\cdot10^{16}} A\cdot\nu^{-0.1}\, d\nu = 3\cdot10^{38} \text{ ergs s}^{-1}$$

where R is the distance of the Cygnus Loop and

A is the amplitude of the radio spectrum: $S_\nu = A\nu^x$.

If all this energy is utilized in ionizing hydrogen, then there will be enough power available to ionize 10^{49} atoms/s. Six hundred filaments of length 1 pc and diameter 0.007 pc subtend about (1/10)% of the surface of a sphere with radius equal to 20 pc. Thus, if the filaments are optically thick in the range λ100 to λ915, the hard, non-thermal radiation could produce on the order of 10^{46} ionizations s^{-1}.

We have estimated the number of ionizations needed by computing the number of Hβ transitions for N_e = 200 cm^{-3}, T_e = 20,000°K and then estimating the total number of all Balmer transitions. Assuming that the Lyman line radiation is reabsorbed, the number of ionizations per second is $3\cdot10^{-8}$ cm^{-3}. For a total emitting volume of 10^{54} cm^3, the number of ionizations required is $3\cdot10^{46}$ s^{-1}, i.e. essentially the number available. Thus it seems that there could be enough power from the extrapolated continuum to maintain the

ionization of the filaments. However, it seems doubtful that this is actually the case since the existence of the hard radiation is rather questionable; and even if present, much of its energy will be used to heat the ambient material.

D. Space Distribution of the Radiation

Comparison of Radio and Optical Emission

One of the curious features of the Cygnus Loop mentioned earlier is the approximate coincidence of radio and optical radiation for Source C, while there is hardly any optical radiation from Source A (the brightest part of the Loop in the radio emission). The discussion of the Cygnus Loop presented arguments that this apparent coincidence did not mean that the physical process responsible for each type of radiation was the same. In support of this view, MLH have pointed out that the radio emission generally falls somewhat inside the bright optical counterparts. This is particularly evident on the 408 Mc contour map of Source C of the Cygnus Loop and is corroborated by the present observations (figure 7, p. 45). This type of separation is also present in HB9. A comparison of figures 15 and 19 (Appendix IV) shows that the radio emission has a maximum value inside the brighter optical parts.

The conditions necessary for Hα emission are a high density of hydrogen (e.g. 200 cm^{-3} in the Cygnus Loop filaments, Osterbrock 1958) and a suitable excitation mechanism (believed to be collisional for the older remnants, Minkowski 1958). Synchrotron radiation, on the other hand, relies only on a

flux of relativistic electrons and a magnetic field which has a significant component across the line of sight. These considerations are pertinent to the interpretation of the relation of the two observed types of radiation. If the radio emission does, in fact, fall somewhat inside the Hα regions of high density and strong excitation, then it seems that either the magnetic field and relativistic particles do not penetrate this region, or that the magnetic field lies along the line of sight in the optically bright area. These considerations must be included in any physical explanation of the explosion and subsequent expansion of these objects. More observations, such as higher resolution radio studies and further Balmer decrement measurements, should clarify the relation between the optical line radiation and the continuum.

Shell Structure

Of equal importance is the general structure of supernova remnants. Table VII lists whether a remnant has a uniform optical distribution or shows "limb brightening", characteristic of a spherical shell. The radio emission is indicated either by "double ridges" in the contour diagram (a possible shell) or by "centrally condensed", which indicates that no internal structure is resolved with an $0.^{\circ}8$ beam.

Except for HB21, all remnants listed in Table VII show some type of shell structure. This feature of the larger remnants allows us to make a few qualifications on the conditions surrounding the origin of the magnetic field and rela-

tivistic electrons.

Table VII. Shell Structure of Remnants

Remnant	Optical	Radio
IC443	Shell	Centrally condensed
HB21	Uniform	Centrally condensed
Cygnus Loop	Shell	Shell
HB9	Shell	Double ridges
S147	Small shells	?
CTA1	Shell	Double ridges
W44	?	Shell (Leslie, 1960)

The supernova remnant model described by Hoyle (1960) is completely compatible with a shell structure since both the magnetic field and the energy for the relativistic electrons are derived from the shock front interacting with the galactic field and cosmic ray energy reservoir. However, several authors have criticized this model on the basis of insufficient energy in the case of young remnants such as the Crab Nebula and Cas-A (e.g. MLH). Therefore, let us restrict the discussion to the hypothesis that the field and relativistic electrons originate with the supernova itself. In this case, the presence of a shell structure suggests that the emission of particles or magnetic field takes place over a time short compared to the age of the remnants, and, in addition, that the velocity dispersion of ejected gas is not too large. The restrictions on the duration of emission and

velocity dispersion will depend on the thickness of the shell and initial velocity, but the relative order of magnitude for these quantities should be similar for all shell-type objects.

E. Time Variation of Observable Parameters

Empirical Spectral Index Variation

We come now to the question of evolution. Thus far in our arguments we have not discussed the reasons for believing that the spectral index flattens with age. This hypothesis is suggested by the loose correlation of flatter-type spectra with increasing angular size which is apparent in Table X (Appendix IV). In order to examine the question more closely, the distance to the remnant becomes of critical importance. Only when the distance is known can the angular size give the physical diameter which permits an estimate of the age to be made.

Diameter Determination. Reliable distances are available for only Cas-A, the Cygnus Loop, and the Crab Nebula. To make an order of magnitude estimate of other distances, we introduce the ad hoc assumption that the physical diameter of filaments is constant. This assumption appears satisfactory for the three sources of known distance. We differentiate between the long thin filaments prominent in the Cygnus Loop and the thicker knots of Cas-A. Knots occur also in HB21, in Puppis-A, and in the south-east sector (Source A) of the Cygnus Loop. The knots of Source A are about 3 times

thicker than filaments, but they are about the same size as those in Cas-A.

The measurements which determine the filament sizes are given in Table VIII. Unfortunately, high resolution plates are not available for all the sources, and angular diameter measurements were often made from the 48-inch Schmidt plates. This method suffers from the lack of resolving power inherent in the small scale of the Schmidt telescope. Distances computed from filament sizes are listed in Table X (Appendix III).

On the basis of this first estimate of distance, the diameter (in parsecs) of each remnant has been computed and plotted against the spectral index (figure 9). The open circles represent objects for which distances were derived from optical measurements. The constant filament size hypothesis was used for all objects except Cas-A, the Crab Nebula, Kepler's and Tycho's supernovae, and the Cygnus Loop. Distances of these sources were inferred from radial velocity and proper motion observations (Minkowski, 1958, 1959).

The plotted points lie in the neighborhood of one of the two straight lines drawn. Tentatively, the right hand line is identified with type II supernovae and the left hand line with type I supernovae. This classification does not contradict any of the known arguments put forth about population membership (e.g. Minkowski, 1958). The correlation of figure 9 suggests that a supernova remnant forms with a steep

Table VIII - Filament Diameters

Source	Diameter (sec. of arc)	Distance (pc)	Diameter (pc)	Reference
Cas-A				
Knots	1 to 2	3400	0.016 to 0.033	Minkowski (1959)
Crab Nebula				
faint, thin	1.6±0.6	1100	0.0085±0.003	Measured from reproduction of Baade's 200" plate, (1956)
bright, thick	4.6±0.6		0.024 ±0.003	
Cygnus Loop				
Filaments	1.8	770	0.0067	Osterbrock's measurement of 100" plate (1958)
Knots	5.0±1.8		0.018 ±0.006	48" Schmidt print
Adopted Size				
Filaments			0.007	
Knots			0.02	

The ± values are an indication of the range of measurements for different filaments.

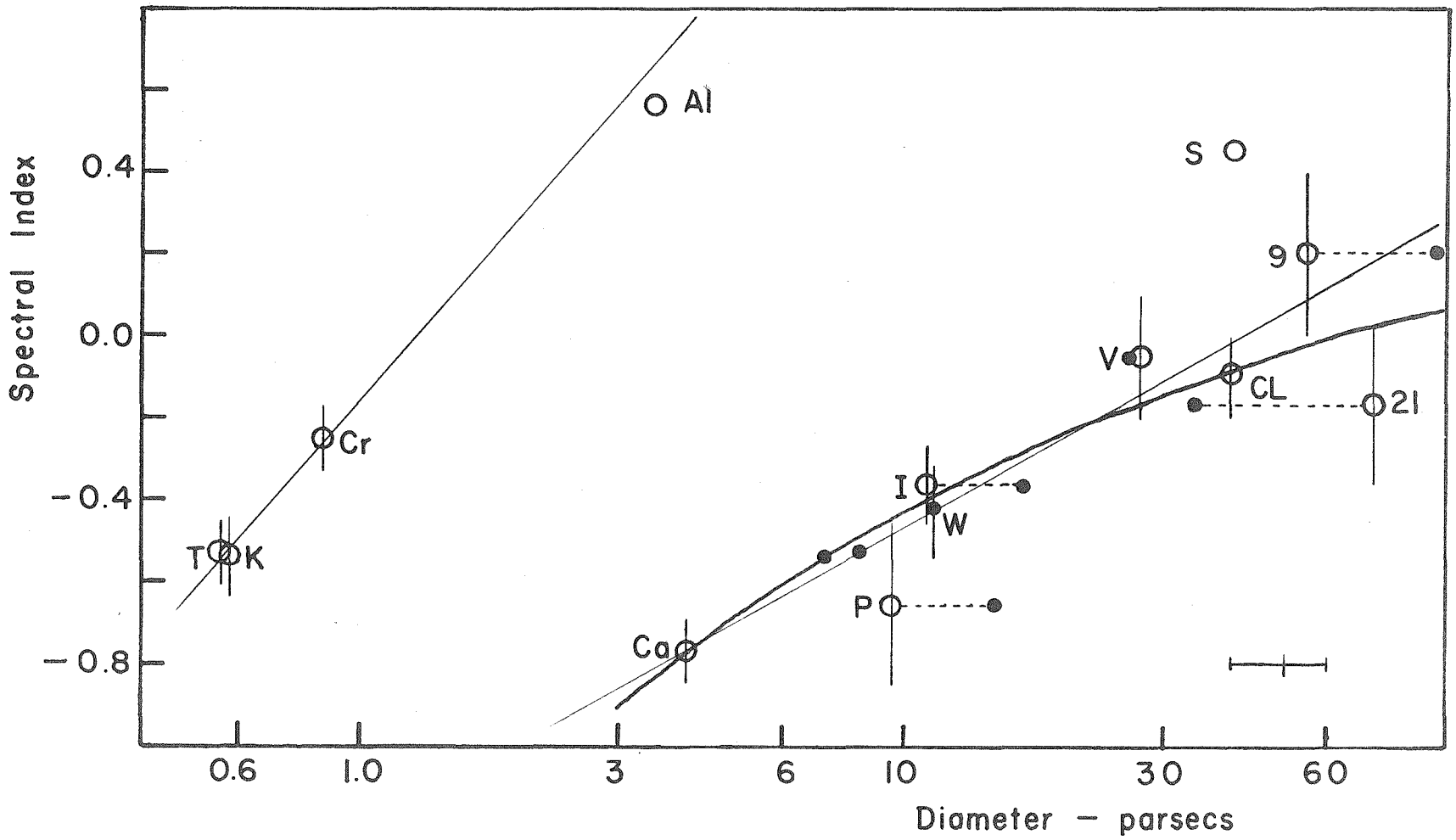

Figure 9 Relation between Spectral Index and Size of Supernova Remnants. Open circles denote that diameters depend on "optical" distance determinations while the smaller dots indicate the use of Shklovsky's method. The horizontal line in the lower right corner shows the magnitude of a ±20% error in the diameter. Source abbreviations are defined in the caption under Figure 10.

spectrum and small diameter. As it evolves, its path will stay close to the line drawn; the spectral index decreases as the remnant expands. This hypothesis is based on the empirical grouping of points along a line rather than a scattering of points throughout the plane.

The spectral index would not be expected to change without limit, and therefore we have put an exponential curve through the points of Cas-A and the Cygnus Loop. The somewhat arbitrary condition of this curve is that as r approaches infinity, x approaches +0.5. The asymptotic behavior for r close to zero has not been fixed, as we have no knowledge of the spectral index for very young remnants. The equations associated with type II supernovae are then found to be:

$$x = 0.765(\log d) - 1.26 \quad \text{straight line fit} \tag{1}$$

$$x = -1.96\, d^{-0.32} + 0.5 \quad \text{exponential fitted to the form: } x = a \cdot \exp(-b \cdot \log d) + 0.5. \tag{2}$$

For future reference, we express these equations in the form:

$$r(\text{parsecs}) = 10^{2-\beta/3.06} \tag{1a}$$

$$r(\text{parsecs}) = 306\,\beta^{-3.12} \tag{2a}$$

where x = spectral index

d = diameter (parsecs)

r = radius (parsecs)

$\beta = 2\gamma = 2(1-2x)$

Shklovsky's Distance Determination. Shklovsky has recently published two papers on supernova remnants (Shklovsky, 1960a, 1960b). First, he has formulated an expression for the radio emission of a supernova remnant as a function of size. Then, in the second paper, he applies this principle to obtain the distance of particular remnants. The basic assumptions of Shklovsky's approach are:

a) Synchrotron radiation is responsible for the observed radio emission.

b) Initial conditions do not vary significantly from remnant to remnant. For this reason, the discussion is restricted to type II remnants.

c) The magnetic field strength is given by $H = H_o(r_o/r)^2$.

d) The energy of the relativistic electrons is degraded chiefly by the expansion term in Fermi's statistical acceleration expression. This is given by $dE/dt = -(V/r)E$ (i.e., each electron loses the same percent of its energy). From this, Shklovsky derives $K = K_o(r_o/r)^{\gamma-1}\ (r_o/r)^3$.

K is the amplitude of the electron energy distribution: $dN(E) = KE^{-\gamma}dE$.

r_o is the radius at some initial time.

K_o and H_o are K and H evaluated at that time.

V is the velocity of expansion.

The power emitted by a remnant due to the synchrotron mechanism is given to sufficient accuracy by:

$$F_\nu \propto (2.8\cdot10^8)^{\frac{\gamma-1}{2}}\, r^3 K H_\perp^{\frac{\gamma+1}{2}}\, \nu^{\frac{1-\gamma}{2}} \qquad (3)$$

energy radiated $s^{-1}(c/s)^{-1}$ at ν

For an exact expression, see Ginzburg, 1958 (equation 21, p. 354).

When K and H are replaced by the expressions given above,

$$F_\nu(\beta,r) \propto H_o K_o r_o^3 (2.8\cdot10^8 H_o/\nu)^{\beta/4 - \frac{1}{2}} (r_o/r)^\beta \qquad (3a)$$

We shall be concerned mostly with the surface intensity rather than the emission of the whole nebula. Therefore, the above equation is expressed as:

$$(S_\nu/\phi^2) \propto (F_\nu/4\pi r^2)$$

$$\propto \left\{H_o K_o r_o^3 \left[\frac{2.8\cdot10^8 H_o}{\nu}\right]^{-\frac{1}{2}}\right\}\left\{\left[\frac{2.8\cdot10^8 H_o}{\nu}\right]^{1/4} r_o\right\}^\beta r^{-(\beta+2)} \qquad (4)$$

or $$(S_\nu/\phi^2) = \frac{A_\nu B_\nu^\beta}{r^{\beta+2}}$$ where $$B_\nu \equiv \left[\frac{2.8\cdot10^8 H_o}{\nu}\right]^{1/4} r_o$$

S_ν = flux density arriving at the earth $(Wm^{-2}(c/s)^{-1})$.

ϕ = angular radius of the remnant.

R = distance to the remnant.

At this point Shklovsky substitutes $r = R\phi$ to calculate the distance from the observed surface intensity and angular size. Unfortunately, individual values of spectral index were not available to Shklovsky and he assumed that all the older remnants had a spectral index of -0.5. Thus he was able to lump the constants A_ν and B_ν^β together and use only the Cygnus Loop as the normalizing condition. Using our

values of spectral index, we have recomputed distances on the basis of equation 4. The Cygnus Loop and Cas-A serve as the normalizing conditions necessary to determine A_ν and B_ν. These distances are listed in Table X together with Shklovsky's original values. On the basis of the revised distances, diameters have been computed and these values are shown as small dots in figure 9.

Surface Intensity. We are now in a position to express the surface intensity as a function of β only. This is effected by utilizing the empirical relation between spectral index and radius which was found earlier (eq. 2). It must be realized that this introduces the evolutionary hypothesis whereas Shklovsky's model predicts that the spectral index is constant with age. (Shklovsky derived this result from the assumption that the electron energy distribution is mainly affected by expansion losses which leave the form of the distribution unchanged.)

If the linear relation between log d and spectral index were adopted, the log surface intensity would be a second degree function of spectral index:

$$\log(S_\nu/\phi^2) = (\log A - 4) + (\log B - 4/3)\beta + \beta^2/3.06$$

In practice, this has the disadvantage of diverging for small values of β (inverted spectra). In order to obtain the correct asymptotic behavior for large radii, the exponential form of the relation has been chosen (eq. 2a).

We take the logarithm of eq. 4:

$$\log(S_\nu/\phi^2) = \log A + \beta \log B - (\beta + 2) \log r$$

and from eq. 2a we replace r:

$$\log(S_\nu/\phi^2) = \log A + \beta \log B - (\quad + 2) \log \left[\frac{306}{\beta^{3.12}}\right] \quad (5)$$

An average curve of this form was determined by using Cas-A and the Cygnus Loop as calibrators. The values of the constants found in this manner are log A = +3.13 and log B = +0.25. Figure 10 plots the 960 Mc surface intensity for the remnants as a function of β. Equation 5 is drawn on the graph to demonstrate one particular way in which the surface intensity may depend on the spectral index. However, the important fact is that some type of correlation exists between low surface intensity and flat spectra. This observation supports the hypothesis made earlier that the spectral index changes with age.

The relation between diameter and spectral index shown in figure 9 implicitly assumes that the remnant expands with time. The equivalent assumption necessary to interpret figure 10 is that the surface brightness decreases with age. Both of these assumptions are certainly valid for the later stages of a supernova remnant, although the second one may be unjustified for a very young object. However, it is important to realize that the results of figure 10 do not depend on a knowledge of the distances of the remnants, as was the

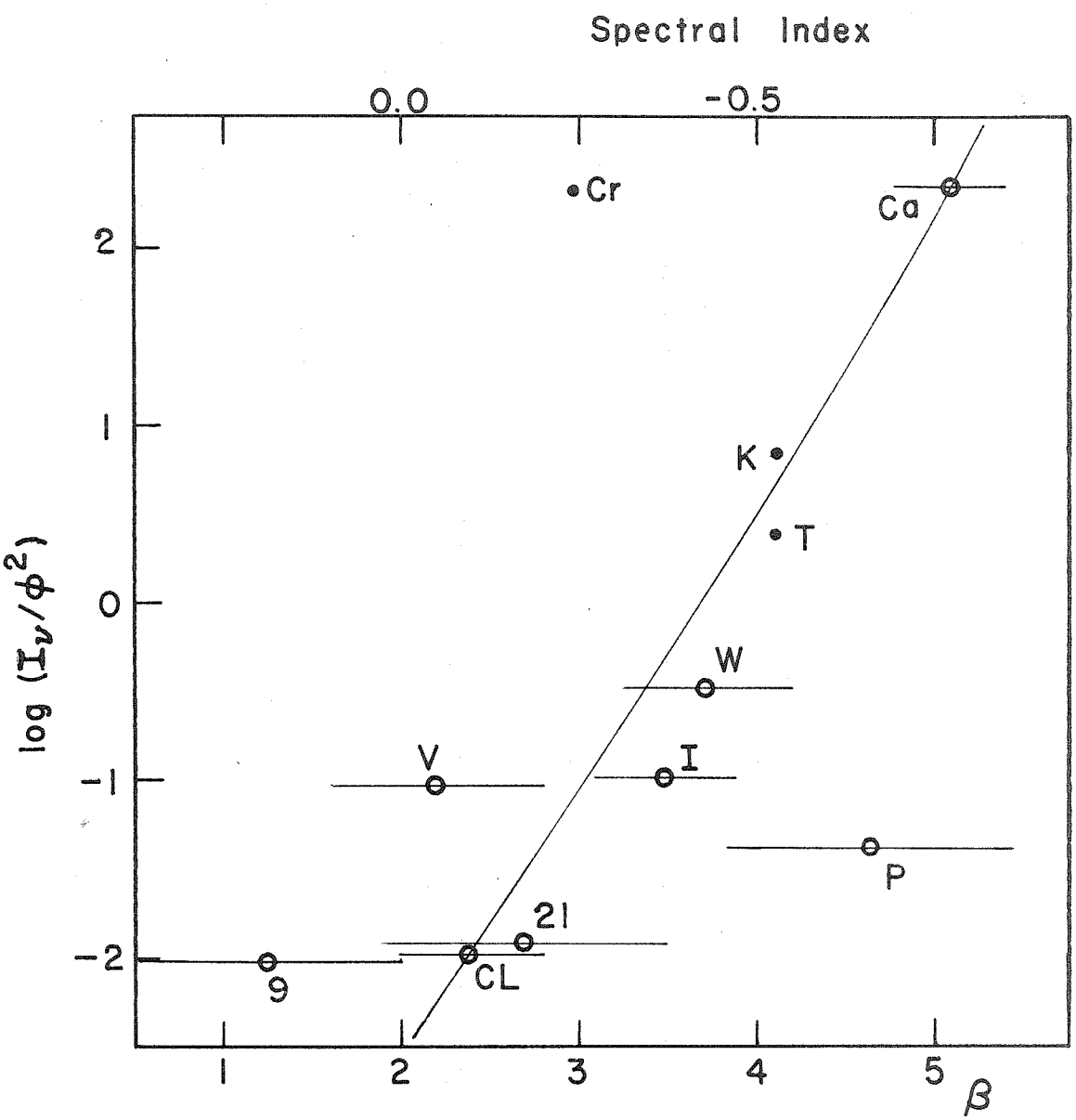

Figure 10 Relation between Surface Intensity and Spectral Index of Supernova Remnants. The abbreviations used in figures 9 and 10 are defined as follows.

T - Tycho's Supernova	A1 - CTA1
K - Kepler's Supernova	Cr - Crab Nebula
P - Puppis A	Ca - Cas A
I - IC443	CL - Cygnus Loop
W - Westerhout 44	21 - MB21
V - Vela X	9 - MB9
S - Shajn 147	

case in figure 9. Thus, each of the independent correlations suggests that the spectral index becomes more positive with age.

Remarks. Shklovsky has argued that the surface intensity of remnants with steep spectra will decrease more rapidly than the intensity of remnants with flatter type spectra. This follows from the dependence of the emission on $H^{\frac{\gamma+1}{2}}$ and the assumption that $H = H_o(r_o/r)^2$. Observational selection will discriminate against sources of low surface brightness and therefore one should find a correlation of flat spectra with old remnants. This process should be most effective in reducing the population of sources lying to the right of the average lines in both figure 9 and figure 10 (steep spectra together with large diameter or low surface intensity). However, this selection should not discriminate against flat spectra concomitant with small diameter or high surface intensity (significantly to the left of either line). The observations to date do not place any remnants in these regions. Therefore, the absence of small, bright objects with flat spectra is the only empirical evidence which favors the time dependence of spectral index, rather than Shklovsky's interpretation of a constant spectral index.

If there did exist a young remnant with a flat spectrum, Shklovsky would predict that the expansion should not decrease its surface intensity as fast as a similar expansion for a

remnant with a steeper spectrum. Therefore, a longer lifetime of high surface intensity would be expected for objects with flat spectra. Assuming a creation function independent of spectral index, one would thus expect to observe more high surface intensity remnants with flat spectra than with steep spectra; actually, the contrary seems to be true.

Predictions. If the remnants do follow the evolutionary lines of figure 9 rather than expanding with constant spectral index, there should be a secular decrease of spectral index which would be most noticable for young, rapidly expanding remnants. From equation 2 the annual change of spectral index for Cas-A is calculated to be 0.0015. For the Cygnus Loop the expected change is 10^{-6} per year. Although these changes are very small, in twenty years the spectral index of Cas-A should change by 0.03. It is possible that this variation could be measured by refined techniques. Extrapolating back in time for Cas-A yields a lower limit of $\Delta x = +0.3$ for 200 years. This would place Cas-A at the steep end of the spectral index distribution when it was very young. (Of course, the empirical nature of equation 2 limits its usefulness, since the extrapolation must become invalid for very young remnants.)

The changing spectral index will also make a small correction to Shklovsky's calculation of the rate of emission decay. He predicts a secular decrease of the flux density of 2% a year for Cas-A. A recalculation of this quantity

which includes a changing spectral index gives about 1.3% a year; a value which is not significantly different from the original prediction.

If the magnetic field strength in a remnant is inversely proportional to the square of the radius as Shklovsky has suggested, then in principle the empirical relations found here enable an estimate to be made of the magnetic field strength. When equation 5 is fitted to the type II remnants, Cas-A and the Cygnus Loop, the constant term B is evaluated. This yields:

$$\log B = +0.25 = \log \left[\left(\frac{2.8 \cdot 10^8 H_o}{\nu} \right)^{1/4} r_o \right]$$

Unfortunately, H_o has little effect on the value of B; and B itself is not well determined by the empirical fitting of equation 5. Therefore, the H_o derived by this process (35 gauss for r_o = 1 parsec) is of little practical significance.

Physical Implications of the Time Variation of Spectral Index

The physical explanation of the proposed spectral index variation poses a difficult problem. The well-known relation between the spectral index of the radiation, x, and the exponent of the electron energy distribution, γ, is given by $\gamma = (1 - 2x)$. Thus, when a power law of the form $N = \text{const } E^{-\gamma}$ is assumed for the number of electrons with energy, E, the spectral index of the radio emission uniquely

determines γ. If the radio spectrum does flatten with age, the energy distribution of the electrons responsible for this radiation must alter in the sense of an ever decreasing relative number of low energy electrons. Although we have no completely satisfacory explanation for this behavior, two alternatives are considered: a selection effect which would separate particles of different energies; and a temporal effect which would modify the energy spectrum by a change of the energy loss mechanism for the relativistic electrons.

Space Separation of Particles. The first of these possibilities could be implemented by a method suggested by Bolton and Roberts (private communication). If a relative concentration of high energy electrons could be progressively collected in a region of strong magnetic field, this distribution would contribute more of the radio emission than the weaker field region which would contain a preponderance of low energy particles. In this model, the region of strong field is the outer shell of the remnant while the comparatively low emission region of the center is assumed to have a weaker field.

Calculations have been made to determine whether the differential radius of gyration of low and high energy electrons is sufficient to allow the high energy particles to escape the central weak field region and become trapped in the outer shell. This calculation assumes a magnetic field with a roughly circular structure. The orbital radius (in

centimeters) of a relativistic electron spiraling in a uniform magnetic field is given by:

$$r = (E/300\ H)\sin\theta$$

where E is the energy in electron volts, H is the magnetic field strength in oersteds, and θ is the angle between the particle trajectory and the magnetic field (Ginzburg, 1958). The relation between the electron's energy and effective radiation frequency is also given by Ginzburg:

$$\nu_{max} = 2.4 \cdot 10^6 H_\perp (E/mc^2)^2$$

where $H_\perp$ is the component of magnetic field strength perpendicular to the particle's direction of motion. From the above two equations, the orbital radius of electrons responsible for various frequencies of emission may be calculated. A few values are given in Table IX.

Table IX. Radius (parsecs) of Electron Orbits

Frequency (c/s)		$H = 10^{-6}$	$H = 10^{-4}$
10^7	low frequency radio	$4 \cdot 10^{-6}$	$4 \cdot 10^{-9}$
10^{10}	high frequency radio	10^{-4}	10^{-7}
10^{15}	optical	$4 \cdot 10^{-2}$	$4 \cdot 10^{-5}$

Since the radii of the observed type II remnants vary from 2 to more than 20 parsecs, it is obvious that even for weak fields and high energy electrons, the size of the electron orbits is several orders of magnitude less than the size

of the supernova remnants. Although this particular separation mechanism is not adequate to produce the required separation of particles, it is possible that eventually some method of selecting only a part of the total electron energy distribution could be used to explain the flattening of the radio spectrum with age.

Change of Energy Loss Mechanism. The second alternative proposes that the degradation mechanism responsible for the major loss of an electron's energy changes with time. Ginzburg (1958) has examined the effect of various types of energy loss on the electron energy distribution. The general solution to this problem is not known in analytic form. Ginzburg treats the "stationary" case of the effect of certain loss mechanisms on the energy distribution of an assumed exponential injection spectrum. Although this treatment excludes the type of behavior of interest to us (time variation of the energy distribution), the conclusions reached by Ginzburg are of qualitative interest.

The losses may be classified by the degree of energy dependence. Ginzburg's treatment considers a general quadratic expression of the form:

$$dE/dt = -a + \alpha E - bE^2 \qquad (6)$$

where E = the energy of the electron; a and b are ≥ 0. Under the assumptions of an exponential injection spectrum ($q = \text{const } E^{-\gamma_o}$), and no time dependence of the electron

energy distribution, Ginzburg demonstrates that the index of the resulting electron energy distribution, γ_{eff}, depends on which term of equation 6 predominates. If dE/dt is independent of energy, $\gamma_{eff} = \gamma_o - 1$; if the energy loss is a linear function of the energy, $\gamma_{eff} = \gamma_o$; and when dE/dt is determined by the bE^2 term, $\gamma_{eff} = \gamma_o + 1$. The quadratic term accounts for synchrotron radiation and inverse Compton losses. Collision bremstrahlung, Fermi statistical accelerations ($\alpha > 0$) and losses due to the general expansion of the remnant are linear in their energy dependence and thus would not change the injection spectrum. Finally, the loss of energy due to ionization of the ambient medium is a function of log E and is adequately approximated by the constant term of equation 6.

Since Ginzburg has considered only the case of a stationary energy distribution, he did not estimate the time necessary to modify γ_o to γ_{eff}. Clearly, the rapidity with which the energy distribution responds to a change of energy loss mechanism will depend on the magnitude of the coefficients of equation 6. However, in the case of supernova remnants, the response time is unimportant. If the absolute magnitude of the loss is small, the remnant will have a longer lifetime in which to respond to any change. Therefore the pertinent time scale is determined by the time required for a significant change of the physical parameters.

The energy loss for each process mentioned above has

been computed as a function of energy and the appropriate variables. Figure 11 shows log(dE/dt) as a function of log E. The steepest lines represent synchrotron radiation losses for magnetic field strengths indicated: $dE/dt \propto E^2H^2$. Expansion losses are indicated by broken lines: $dE/dt \propto (V/r)E$; V = the velocity of expansion, r = the radius of the remnant. The upper line, labelled "C" is appropriate for Cas-A and the Crab Nebula while the lower one, "CL", applies to objects such as the Cygnus Loop. The dashed lines give estimates of collision bremstrahlung losses for densities indicated: $dE/dt \propto nE$; n = density of hydrogen. The nearly flat dotted lines represent losses from ionizing collisions with ambient hydrogen atoms: $dE/dt \propto n \cdot \log E$.

The energy range of 10^9 to 10^{10} ev is primarily responsible for the radio emission at 1000 Mc. Examination of this energy range in figure 11 shows that unless the field is very strong ($H > 10^{-3}$ oersteds) or the density is very high ($n > 1000$ cm^{-3}), the dominating energy loss will be that of expansion. However, if this mechanism were greatly reduced (which would be the case, for example, if large parts of the shell were ejected as coherent pieces with no internal expansion), the parameters could easily allow a change of energy degradation from synchrotron radiation to collision bremstrahlung. This type of behavior could occur if the density in the shell increased or if the magnetic field strength decreased. A qualitative calculation

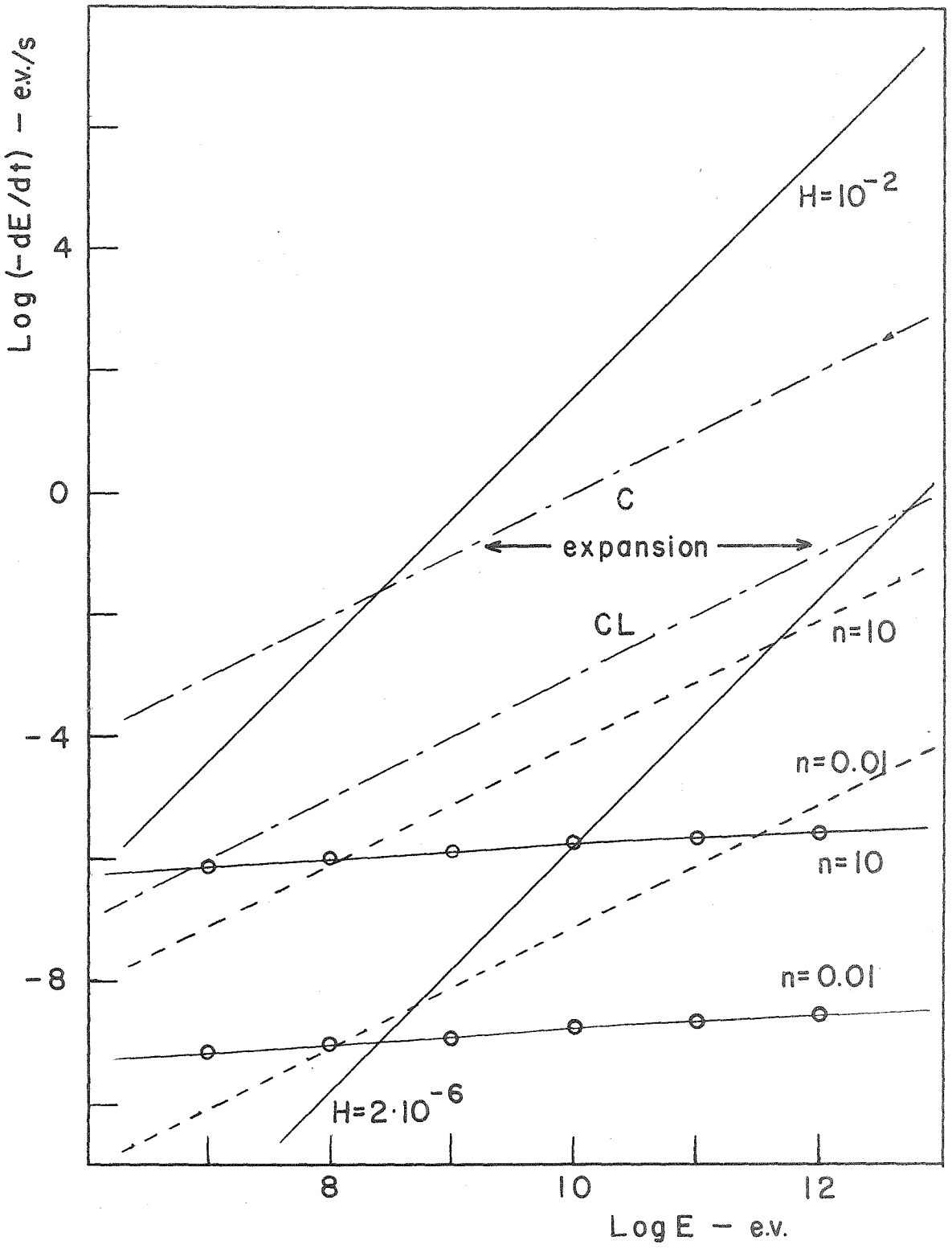

Figure 13 Energy Losses of Relativistic Electrons.

will not be attempted since this treatment is based on the simplifying assumptions of no time dependence and an exponential injection spectrum. This discussion is presented to demonstrate that a time variation of parameters such as velocity of expansion, magnetic field intensity, and ambient density could lead to a changing radio spectrum. A decision of whether or not such a variation actually occurs must wait until a solution of the time dependent equation is found and the injection spectrum is known.

Future Lines of Investigation

Very Young Remnants. From an astrophysical point of view, the most interesting aspect of supernovae concerns the outburst itself and the causes of it. This type of problem arises in the course of stellar evolution and is of primary importance in theories of nucleosynthesis. However, as there have been no known supernova outbursts in our own galaxy during this century, only very distant supernovae can be studied, and the techniques of radio astronomy are as yet unable to provide any information on individual objects of distant galaxies. Thus, although the present type of study does not pertain directly to observed outbursts, it may lead to knowledge of very young remnants and eventually it may permit an extrapolation of the electron energy distribution and magnetic field configuration back to a stage immediately following the initial outburst.

A related problem, that of cosmic rays, is probably con-

nected with one or all of the supernova stages. The outburst may generate cosmic rays, and the radio emission itself is evidence of relativistic electrons existing in the remnants. The similarity of the energy spectra of these electrons to the spectrum of the cosmic rays arriving at the earth supports the contention that some sort of relationship exists between them. In this connection, it should be noted that the cosmic ray energy distribution is very similar to that of the electrons in young, small remnants rather than to the distribution existing in the older remnants. Thus, if supernova remnants are the origin of part of the cosmic ray spectrum, the initial stages would be the most likely time for the generation of cosmic rays.

Kepler's and Tycho's Supernova Remnants. The radio observations of these remnants do not determine which type of supernova they were. Baade (1943, 1945) has classified them as type I on the basis of reconstructed light curves. This interpretation is supported by the relatively small dispersion of radial velocities in the remnants (Minkowski, 1959). However, considerations of the radio nature of these objects suggest a closer similarity to type II remnants than would have been expected. In particular, the radio surface brightness seems to be more characteristic of type II remnants than of the Crab Nebula (i.e. figure 10). Furthermore, if they were type II objects, the observed radio surface brightness would allow the distance to be calculated by the "revised Shklovsky" method which is normalized by the type II remnants

Cas-A and the Cygnus Loop. These distances are listed in parentheses in Table X (Appendix III), and lead to diameters which satisfy the type II correlation with spectral index (the two unlabelled dots near Puppis A on figure 9). The distances required for this interpretation are ten times greater than the presently accepted values.

Since the differences between the radio surface brightness of type II and type I remnants is still uncertain, it is possible that the radio observations may not be discordant with the type of supernova as defined by the light curve. However, the radio similarity of Kepler's and Tycho's supernova remnants to type II remnants seems well established as this same feature has been noted by Biraud, Lequeux, and Le Roux (1960).

Association of Supernova with Early-Type Stars. The possible confusion between H II regions and supernova remnants will become especially interesting if hybrid objects exist. Öpik (1953) and, more recently, Shklovsky (1960b) have suggested that supernova remnants should occur in OB associations, since the most massive (and hence most rapidly evolving) stars are often found there. Shklovsky has suggested that the Vela X complex may be an example of this, and also that the non-thermal emission from the Orion Nebula region could be due to an old supernova remnant. One is tempted to add the Rosette Nebula to this list. This nebula has a well defined shell structure and could prove to be a hybrid object which exhibits non-thermal radiation together

with free-free emission from hydrogen ionized by nearby early-type stars.

The Variation of Spectral Index. Since the evolutionary hypothesis depends on the non-existence of small bright objects with flat spectra, an effort should be made to find such objects and distinguish them from H II regions. Probably this would best be accomplished by the comparison of high resolution galactic surveys at several frequencies.

Finally, a satisfactory mechanism has yet to be found for the observed flattening of the spectra with age. The suggestion of a change in energy degradation for the relativistic electrons must successfully explain why expansion losses do not dominate other types of loss if this argument is to be used to describe the mechanism of evolution.

F. Conclusion

The present work is an attempt to measure spectral indices and to consider the implications of their distributions. The intrinsic spread of the spectral index distribution for non-galactic sources seems to be characterized by a width, $\Delta x = 0.5$, which includes 75% of the sources. The galactic sources have a range in spectral index roughly twice as large as this, and since these objects are more completely identified, a correlation of spectral index with age has been possible.

The interpretation of the spectral index-age correlation is considered on the basis of the synchrotron process. If

this correlation is valid, and if the synchrotron process is the correct mechanism for non-thermal sources, then we may expect to find some sort of similar correlation for the external galaxies. This has not been possible with the present data, since our limited accuracy does not allow us to resolve sufficiently the relatively narrower range of spectral indeces found for the external galaxies. Furthermore, only recently have the optical identifications become available in suitable numbers to make a correlation feasible. It seems unlikely that exactly the same correlation will be found for galaxies as for supernova remnants. The size and probable time scales involved differ by orders of magnitude. However, the radio evolution of galaxies may be reflected in a spectral index variation similar to that described for supernova remnants and, if the physical size is not a suitable parameter, some other physical variable may give the desired result.

Appendix I

Calculation of Expected Free-Free Radio Emission from Optical Observations

a) Source C of the Cygnus Loop

This calculation of free-free emission is based on the observed surface brightness of Hα measured by Chamberlain (1953b). In order to find the ratio of free-free emission in the radio continuum to the Hα line emission, we make the usual assumptions:

1) the optical depth is small at 1000 Mc and also in the Hα line, but large for Lyman line radiation;

2) the Rayleigh-Jeans approximation of the Planck function is valid for computing the free-free emission at 1000 Mc;

3) the electron temperature is $40{,}000^{\circ}K$ and the electron density is constant throughout the emitting volume;

4) collisional excitation is responsible for the ionization (if radiative excitation were responsible for the ionization, b_n would be lowered and the radio emission would be larger by a factor of about 3).

Under these assumptions, the volume emissivity for free-free emission is: (Osterbrock and Stockhausen, 1960)

$$j_{1000} = 4.6 \cdot 10^{-37} N_e N_i T_e^{-1/2} \text{ ergs cm}^{-3} \text{ s}^{-1} (\text{c/s})^{-1} \quad (7)$$

where N_e = electron density

N_i = ion density

T_e = electron temperature

The volume emissivity of Hα is equal to the number of atoms in the n=3 state x the transition probability x hν. Following Aller, (1956), the necessary constants are taken as:

$g_{nn'}$ = 0.757 is the Gaunt factor from Baker and Menzal, (1938).

b_n = 4.0 is the correction for departure from thermal dynamic equilibrium for collisional excitation (Chamberlain, 1953a).

The volume emissivity is then:

$$j_{H\alpha} = 3.06 \cdot 10^{-18} N_p N_e T_e^{-3/2} \text{ ergs cm}^{-3} \text{ s}^{-1}$$

$$= 3.82 \cdot 10^{-25} N_p N_e \text{ ergs cm}^{-3} \text{ s}^{-1}$$

for T_e = 40,000°K and where N_p = the number of protons cm^{-3}.

An equivalent calculation, following Burgess (1958), yields:

$$j_{H\alpha} = 2.77 \cdot 10^{-25} N_p N_e \text{ ergs cm}^{-3} \text{ s}^{-1}$$

We adopt an intermediate value of:

$$j_{H\alpha} = 3.5 \cdot 10^{-25} N_p N_e \text{ ergs cm}^{-3} \text{ s}^{-1} \qquad (8)$$

From Chamberlain (1953b), we take the average value quoted for the surface intensity in Hα of the 3 filaments observed in NGC 6992-5. Chamberlain converted the surface intensities to absolute units by measuring the surface brightness of M32 which was in turn related to the solar surface brightness. The surface brightness for the seven filaments measured is given below in units of 10^{-4} ergs $cm^{-2}s^{-1}$

Filament	Hα
A	39 ± 1
B	22 2
C	25 4
D	24 3
E	19 1
F_1	27 2
F_2	20 2

The average of A, B, and C (the three filaments of Source C), is 28. Correcting this figure for the contribution from N [II], (Minkowski, 1958), gives a surface brightness:

$$\sigma_{H\alpha} \approx 14 \cdot 10^{-4} \text{ ergs cm}^{-2} \text{ s}^{-1}$$

The uncertainties in this value are not dependent on the geometry of the situation, but rather on the intrinsic scatter of values and the difficulties in estimating the effects of resolution. Chamberlain has corrected for resolution, but no estimate of his error is given.

The radio surface brightness may now be computed. If there is no self absorption for the radio or Hα emission, then

$$j_{1000}/j_{H\alpha} = \sigma_{1000}/\sigma_{H\alpha} \quad \text{and}$$

$$\sigma_{1000} = \sigma_{H\alpha} \frac{j_{1000}}{j_{H\alpha}} \quad \text{and from equations 7 and 8,}$$

$$\sigma_{1000} = 14 \cdot 10^{-4} \text{ergs cm}^{-2} \text{ s}^{-1} \cdot \frac{2.3 \cdot 10^{-39} N_e N_i}{3.5 \cdot 10^{-25} N_e N_p} \text{ (c/s)}^{-1}$$

$$= 10^{-20} \text{ W m}^{-2} \text{ (c/s)}^{-1} \text{ (for Ni/Np=1.1)}$$

σ_{1000} is then, the rate of energy flow per m^2 in unit frequency interval at the surface of a filament. To obtain the brightness, or specific intensity,

$$b_{1000} = \frac{\sigma_{1000}}{\pi} = 3.2 \cdot 10\text{-}21 \text{ Wm}^{-2} \text{ (c/s)}^{-1} \text{ str.}^{-1}$$

The surface of the filaments subtends a solid angle, Ω_f, which is estimated by 250 filaments of size 1'.8 x 4'.5.

$$\Omega_f = (250/3282)\cdot(1.8/3600)\cdot(4.5/60) = 2.8\cdot10^{-6} \text{ str}^{-1}$$

The integrated flux density at the earth will then be:

$$S_{1000} = \Omega_f \, b_{1000} = 9\cdot10^{-27} \text{ W m}^{-2} \text{ (c/s)}^{-1}$$

or 4% of the observed 960 Mc flux density of Source C. It is felt that the chief source of error in this calculation enters from the uncertainty in correcting for the resolution of the telescope (f/3.5, 24" Schmidt).

b) Path Length and Emission Measure of Source C

Osterbrock's observations of the λ3727 O [II] doublet line ratio, (Osterbrock, 1958) measure the quantity $N_e T_e^{-1/2}$. If a temperature of 40,000°K is assumed, N_e varies from 40 to 500 cm^{-3} for the seven filaments measured. On the basis of Chamberlain's surface brightness described in the previous section, we may derive a path length necessary to produce the observed surface intensity in Hα. For this calculation we use the average electron density quoted by Osterbrock, (N_e = 200 cm^{-3}), to evaluate j_ν from equation 7. The path length in cm will be:

$$L = \frac{\sigma_{H\alpha}}{j_{H\alpha}} = \frac{14\cdot10^{-4} \text{ ergs cm}^{-2} \text{ s}^{-1}}{14\cdot10^{-21} \text{ergs cm}^{-3} \text{ s}^{-1}} = 10^{17} \text{ cm} = 0.033 \text{ pc}$$

For a distance of the Cygnus Loop = 770 pc, the diameter of the cylindrical filaments is equal to 0.007 pc (Osterbrock, 1958), which would give an "average" or "equivalent" path length of 0.004 pc for each filament. There-

fore, it seems likely that there is some geometrical effect which increases the path length by a factor of about 9; ie. the filaments may be stacked in the line of sight or the apparent filaments may actually be sheets seen edge on. In any event, the calculated emission measure is:

$$EM = N_e^2 \, L = 1330 \text{ cm}^{-6} \text{ pc}$$

c) Free-Free Emission from Regions Optically Invisible

If the ionized hydrogen of the Cygnus Loop is in the form of sheets rather than filaments, one would expect that the apparently vacant areas of the Cygnus Loop could well be sheets of ionized hydrogen seen face on. The emission measure would be too small to allow detection of the Hα radiation on the 48" Sky Survey plates as the path length would be very small. The following calculation gives an estimate of the flux density at the earth from free-free emission in ionized hydrogen which would be at the limit of detection on the E plates of the Sky Survey.

Abell (1960) quotes the following figures:

25.5 to 26 mag per square second of arc for the limit of visibility of the E survey plates;

$2.004 \cdot 10^{32}$ ergs s^{-1} for the total energy output of the sun contained in the spectral bandpass used;

-27.1 as the apparent photo-red magnitude of the sun.

These figures reduced to surface brightness are:

$-27.1 + 2.5 \log(\text{area of sun}) = -11.0 \text{ mag}/\square''$

and

$$\sigma_{\text{photo-red}} = \frac{\text{Energy of sun}}{\text{Area of sun}} = \frac{2\cdot10^{32} \text{ ergs s}^{-1}}{6.087\cdot10^{22} \text{ cm}^2}$$

$$= 3.3\cdot10^{9} \text{ ergs cm}^{-2} \text{ s}^{-1}$$

Therefore, the plate limit is 36.5 mag fainter than the sun and,

$$\sigma_{\text{photo-red}}(\text{plate limit}) = \frac{3.3\cdot10^{9} \text{ ergs cm}^{-2} \text{ s}^{-1}}{4\cdot10^{14}}$$

$$= 8.3\cdot10^{-6} \text{ ergs cm}^{-2} \text{ s}^{-1}$$

However, this figure needs a correction factor of 1.3 since λ6563 (Hα) is reduced 22% by the sensitivity curve of the E plates from the maximum of the band pass which was normalized on the sun. Therefore,

$$\sigma_{H\alpha}(\text{plate limit}) = 10^{-8} \text{ W m}^{-2}$$

Using the ratio of surface brightnesses ($\sigma_{1000}/\sigma_{H\alpha}$) computed earlier,

$$\sigma_{1000}(\text{plate limit}) = 7.3\cdot10^{-23} \text{ W m}^{-2} \text{ (c/s)}^{-1} \text{ and}$$

$$b = \sigma/\pi = 2.3\cdot10^{-23} \text{ W m}^{-2} \text{ (c/s)}^{-1} \text{ str}^{-1}$$

For an area of two square degrees (roughly the area of Source C), the flux density at the earth will be:

$$S_{1000} = b\,\Omega = 2.3\cdot10^{-23}(2/3282) = 1.4\cdot10^{-26} \text{ W m}^{-2} \text{ (c/s)}^{-1}$$

or 5% of the observed integrated flux density of Source C. On the deep red plates taken by Minkowski, this value may be lowered by a factor of 3 or 4. (Abell)

d) Free-Free Emission from HB9

HB9 is barely visible on the E plates while it shows quite well on the deep red plates taken by Minkowski (fig. 19).

The total area of HB9 is about 6 square degrees or:

$$\Omega_{HB9} = 6/3282 = 1.83 \cdot 10^{-3} \text{ str}$$

This is 3 times larger than the area of Source C of the Cygnus Loop and therefore the flux density arriving at the earth would be:

$$S_{HB9} = 4.2 \cdot 10^{-26} \text{ W m}^{-2} \text{ (c/s)}^{-1}$$

or about 2.5% of the observed integrated flux density from HB9. This figure ignores the effect of interstellar absorption of the Hα line intensity. As there are two galaxies visible near the south west edge of the nebula, this assumption should not introduce a large error.

Appendix II

Description of the Cygnus Loop Polarization Experiment

In order to select various components of the radiation, the horn feed of the paraboloid was rotated from night to night. The usual position of the horn accepts radiation with the electric vector along an hour angle circle. In the present experiment, the horn was rotated $\pm 45^{\circ}$ about this position and to one other position 90° west of north. If a sufficient percentage of the radiation were polarized, the intensity of the source should vary as the horn is rotated. Cygnus A, the Crab Nebula, and the Orion Nebula were used as intensity calibrators. However, the measured intensity of a spread source (i.e. the Cygnus Loop) relative to a point source will depend on instrumental effects such as a change of the antenna pattern when the horn rotates. Therefore, the calibrators mentioned above were subordinated to "check sources" and the primary effect sought was a variation of the intensity ratio of Source C to Source B. The results of these observations are shown in figure 12.

Figure 12a plots the intensity (arbitrary scale) of the three calibrators and Source A of the Cygnus Loop as ordinate with the angle of horn rotation as abscissa. 0° corresponds to the electric vector parallel to an hour circle and positive rotation is a clockwise (west of north) rotation on the sky. When two observations were obtained at one angle, indicated errors contain both values. Figure 12b gives the ratio

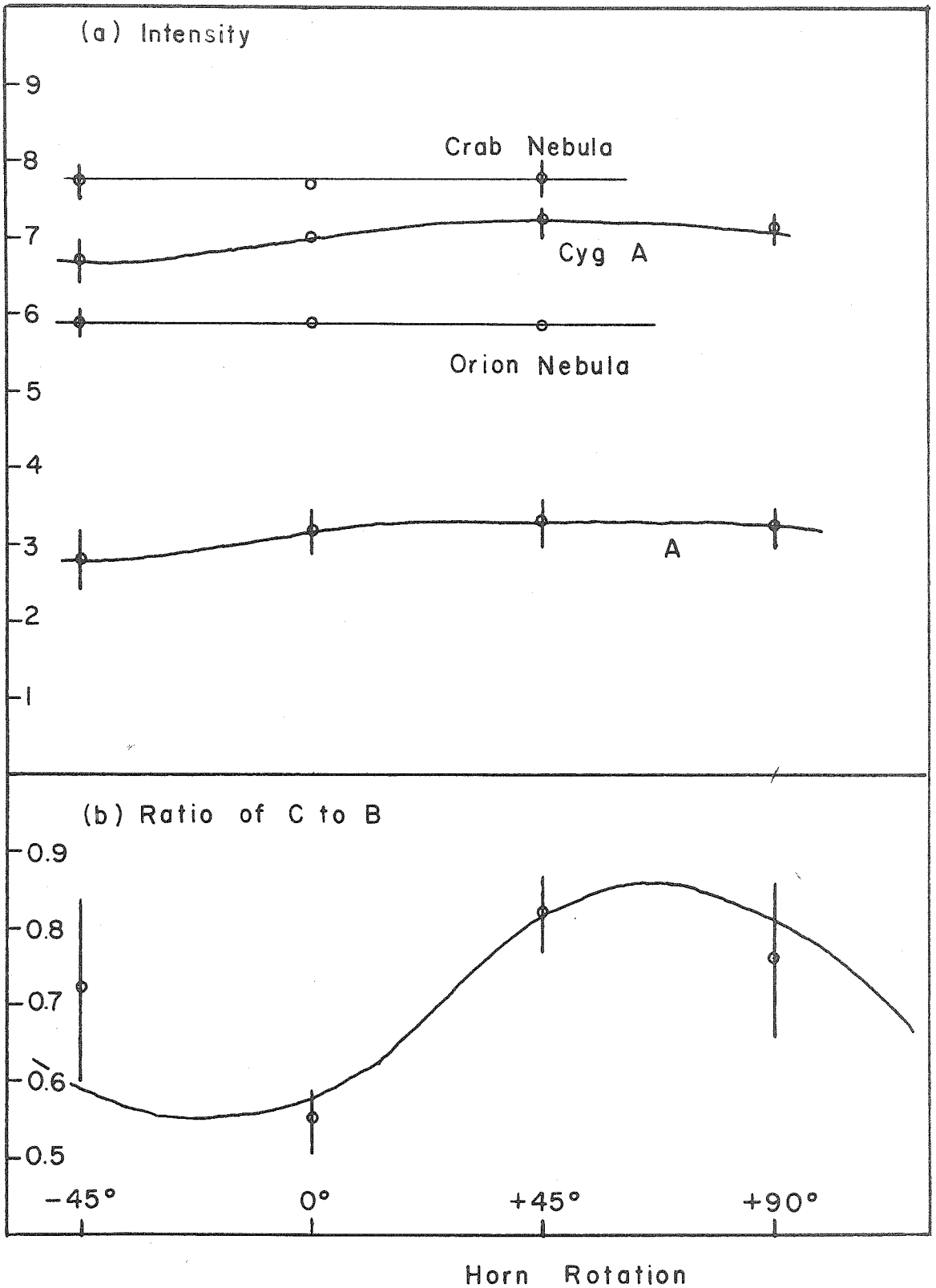

Figure 12 Cygnus Loop Polarization - Intensity.
(a) gives the intensity (arbitrary scale) of source A and three calibrators.
(b) gives the intensity ratio of Source C to Source B.

of intensities of Source C to Source B. Errors shown for each angle are average deviations from the mean of 4 or 5 observations. The results are consistent with a radial field producing about 15% polarization.

From the same experiment, the half-width in the east-west direction of Source A has been measured as a function of horn rotation. This parameter should indicate the presence of any small, strongly polarized source, if its intensity is a significant fraction of Source A. The results are given in figure 13 together with the α and δ beam-widths measured by drift curves of Cygnus A. Once again, the results appear consistent with the proposed polarization; the half power width is at a minimum at approximately the same angle as the intensity is at a maximum (figure 12a). Unfortunately, any instrumental effects are likely to be enhanced in such an experiment where the beam pattern of a point source, Cyg-A, is compared to that of an extended source.

Finally, in September, 1960, another attempt was made to measure the polarization of the Cygnus Loop. The 960 Mc interferometer was used by employing the cross-horn technique described by Radhakrishnan and Roberts (1960). In this experiment, the results suffer from a poor signal to noise ratio since the Loop is resolved by the interferometer and the signal is reduced by a factor of 10 to 100. (The lobe period at the 200-foot spacing is 18 minutes of arc.)

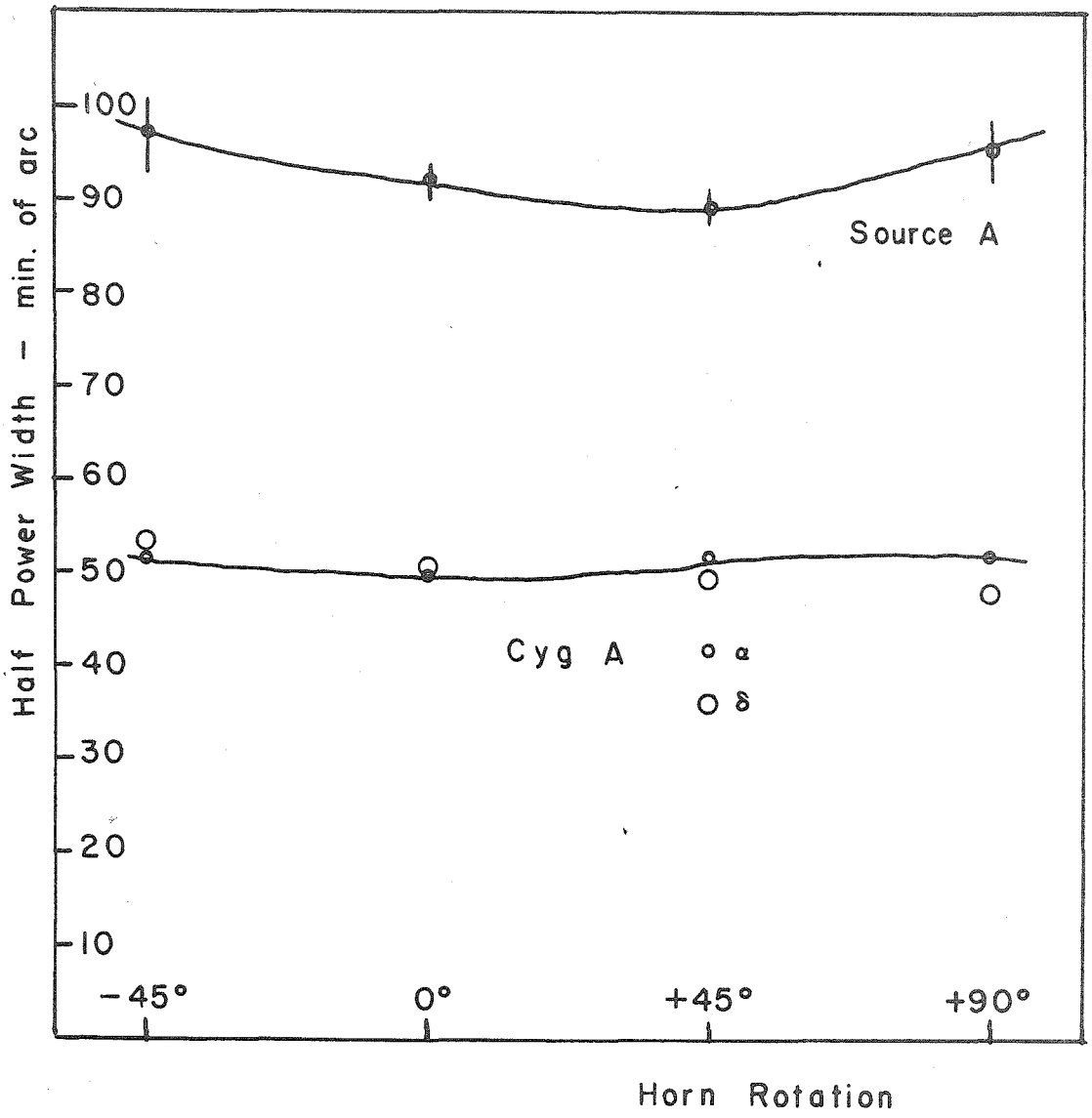

Figure 13 Cygnus Loop Polarization - Resolution.

The half-power width of Source A is given as a function of horn rotation. The right ascension (α) and declination (δ) half power widths of Cygnus A are given for comparison.

Horn rotation is measured by the angle of the electric vector west of north.

Several locations in the Cygnus Loop were observed as one horn was rotated between the parallel and anti-parallel direction. Due to the poor signal to noise ratio, the only possible conclusion is that not more than 30% of the unresolved component is polarized.

The present discussion admits the possibility of a large-scale radial magnetic field existing in the Cygnus Loop, but further observations are needed to demonstrate its reality. Also, it should be remembered that even if the indicated polarization does exist, the stated field direction rests on the assumption of negligible Faraday rotation.

Appendix III.

Table X - Physical Parameters of the Supernova Remnants.

Observed:

Source	Spectral Index	Age (years)	Diameter (min. of arc)	Type* S.N.
Cas A	-0.77±.08	250.	4.	II
Pup A	-0.66±.20		50.x80.	II
Kepler's SN	-0.54±.10	360.	< 2.	I
Tycho's SN	-0.53±.08	400.	5.4	I
W 44	-0.43±.12		22.5	II
IC443	-0.37±.10		48.	II
Crab Neb.	-0.25±.08	900.	2.7	I
HB 21	-0.17±.20		140.	II
Cyg. Loop	-0.10±.10	50,000.	160.x210.	II
Vela X	-0.05±.15		120.x150.	II
HB 9	+0.20±.20		150.x140.	II
S147	+0.45±.8		170.x180.	II
CTA 1	+0.56±.6		90.x100.	I

* The type of supernova is based on Minkowski's (1958) classification or on the inferences of figure 9.

Table X - Physical Parameters of the Supernova Remnants.

Source	Distance Estimates (parsecs) Optical	Filaments	Shklovsky	Revised Shklovsky
Cas A	3400.	3400.	3400.	3400.
Pup A		500.	1800.	780.
Kepler's SN	1000.*			(12,190.)
Tycho's SN	360.*			(5,370.)
W 44			2200.	1,780.
IC443		800.	1700.	1,175.
Crab Neb.	1100.			(5,445.)
HB 21		1800.	1150.	830.
Cyg. Loop	770.	770.	770.	770.
Vela X		700.	1040.	670.
HB 9		1000. 1500.	1300.	2,330.
S147		800.	1100.	(11,400.)
CTA 1		100. 150.		(48,300.)

* Assumes same velocity of expansion as the Crab Nebula.

Distance determinations are described in the text.

Parentheses indicate that the method is inappropriate for that source.

Underlined distances indicate that this value was used for calibration.

Table X - Physical Parameters of the Supernova Remnants.

Source	Adopted Distance (parsecs)	Adopted Diameter (parsecs)	Reference	Power (10^{33} ergs/s) Radio Cutoff	Power (10^{33} ergs/s) Optical Cutoff
Cas A	3400.	4.	Optical	247.	4300.
Pup A	500.	9.5	Filament & Rev. Shk.	0.22	12.
Kepler's SN	1000.	$\leq$0.58	Optical	0.15	32.
Tycho's SN	360.	0.56	Optical	0.05	12.
W 44	1800.	12.	Rev. Shk.	6.5	4720.
IC443	800.	11.	Filament	0.98	1405.
Crab Neb.	1100.	0.86	Optical	10.6	6030.
HB 21	1800.	72.	Filament	5.6	$7.9 \cdot 10^4$
	830.	33.	Rev. Shk.	1.2	$1.7 \cdot 10^4$
Cyg. Loop	770.	40.	Optical	1.6	$5.2 \cdot 10^4$
Vela X	700.	32.	Filament & Rev. Shk.	7.6	$4.3 \cdot 10^5$
HB 9	1300.	50.	Filament & Shklovsky	4.3	$4.3 \cdot 10^6$
S147	800.	40.	Filament	2.0	$3.5 \cdot 10^7$
CTA 1	125.	3.5	Filament	0.03	$2.3 \cdot 10^6$

The radio cutoff is taken as 10,000. Mc and the optical cutoff is taken as 10^{15} c/s.

Appendix IV

Figures 14 to 17 are contour maps of four sources where an arbitrary scale of antenna temperature is given. (Not the same for each figure) The coordinates are for epoch 1950.

Figures 18 to 20 are photographs copied from deep red plates taken by Minkowski with the 48" Schmidt. North is at the top; east is at the left.

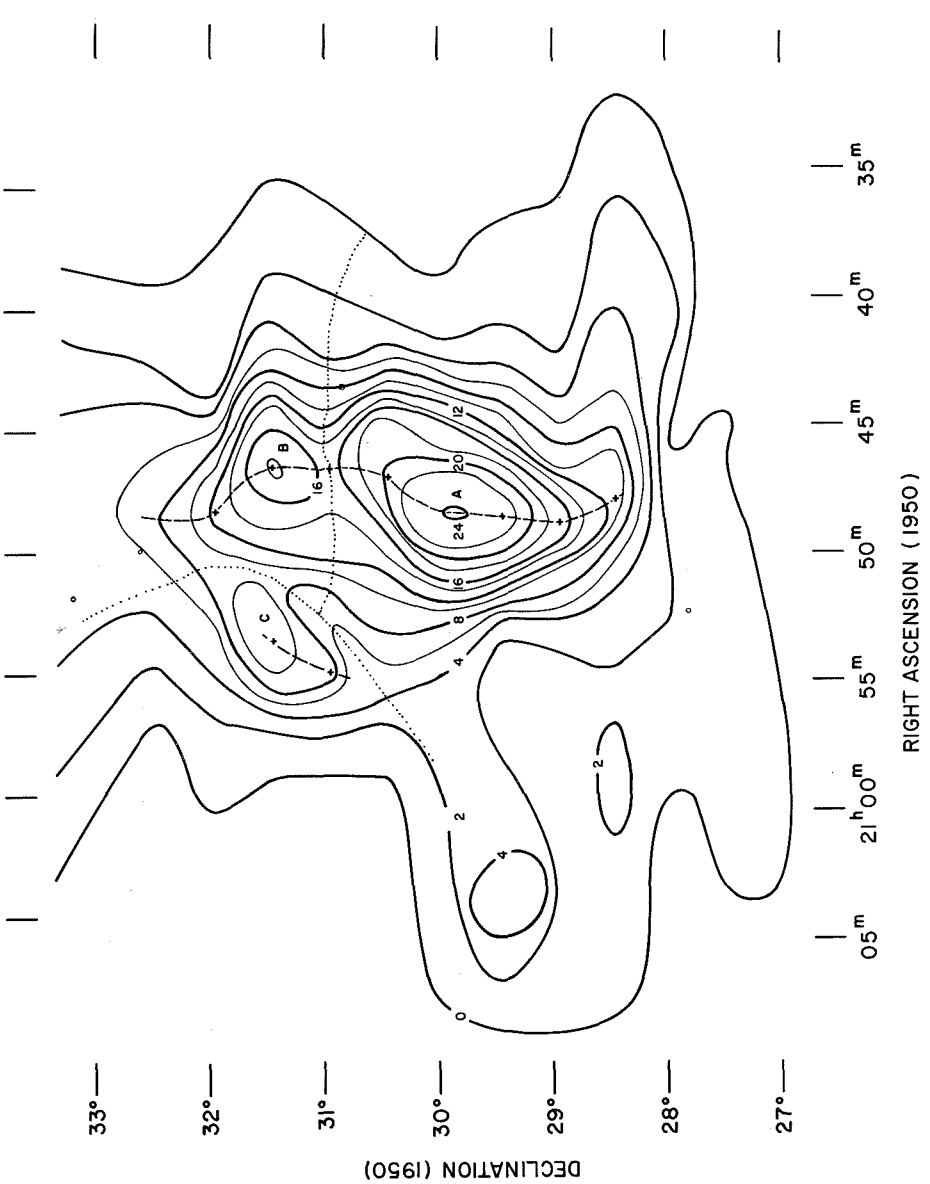

Figure 14 Radio Contours of the Cygnus Loop. Dotted lines show boundaries of Sources A, B, and C.

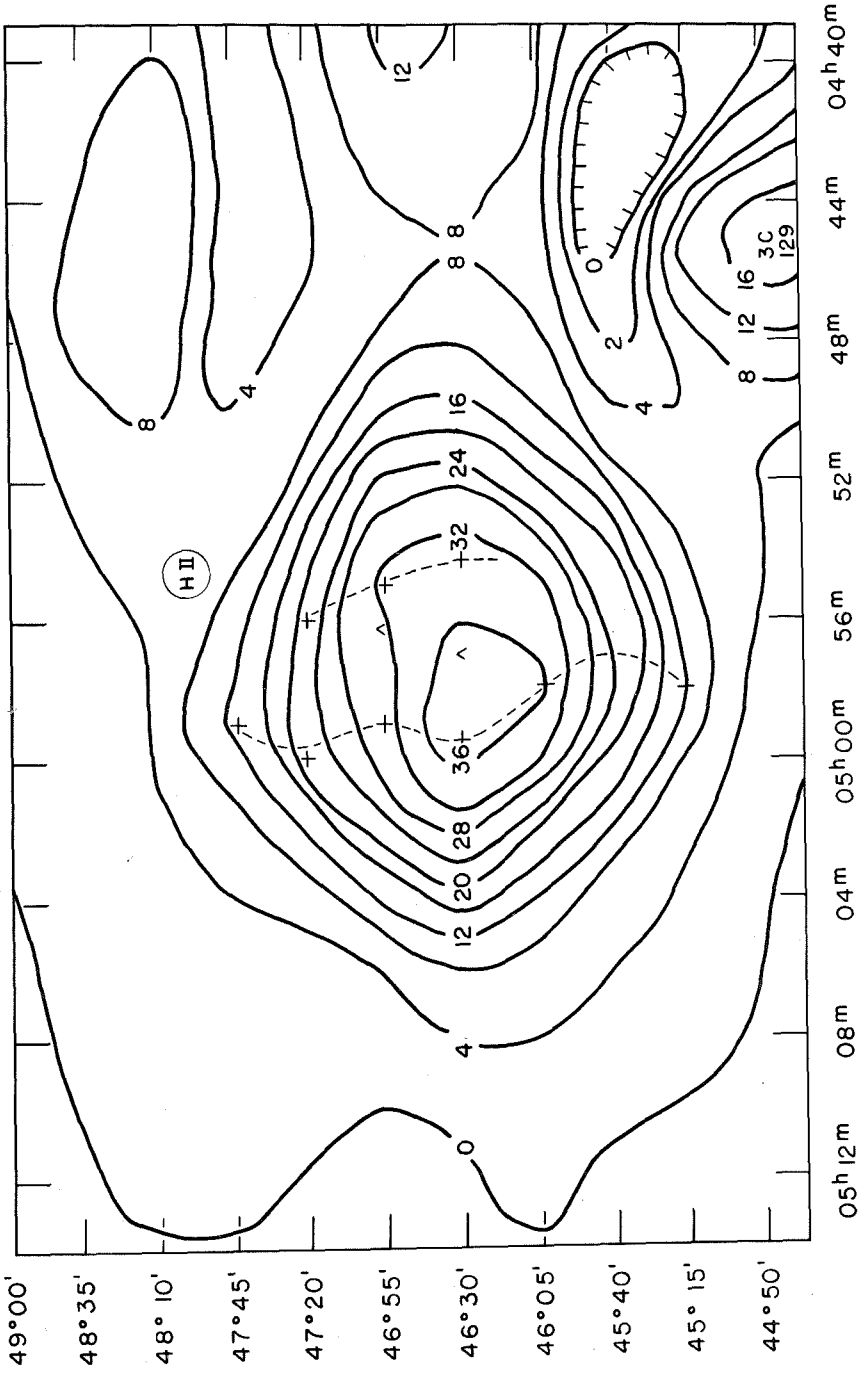

Figure 15 Radio Contours of HB9.

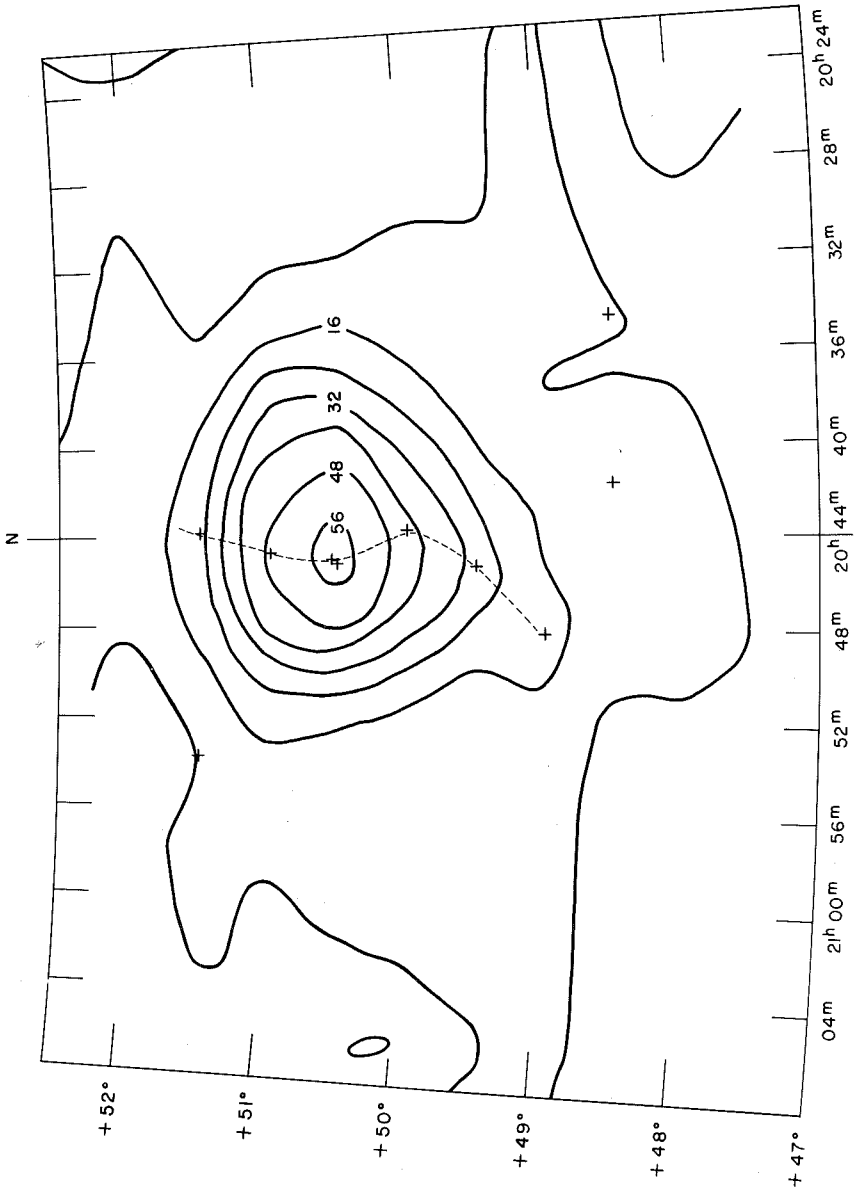

Figure 16 Radio Contours of HB21.

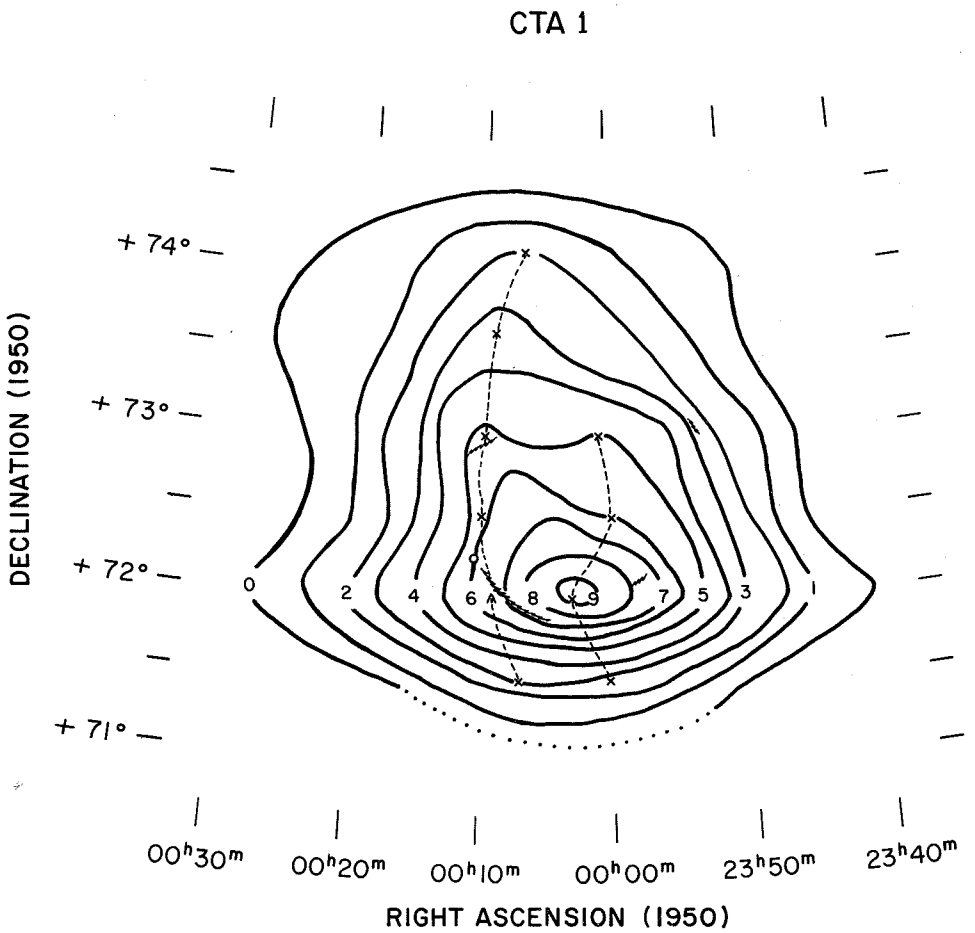

Figure 17 Radio Contours of CTA1. The sawtooth lines indicate the positions of the four faint emission arcs.

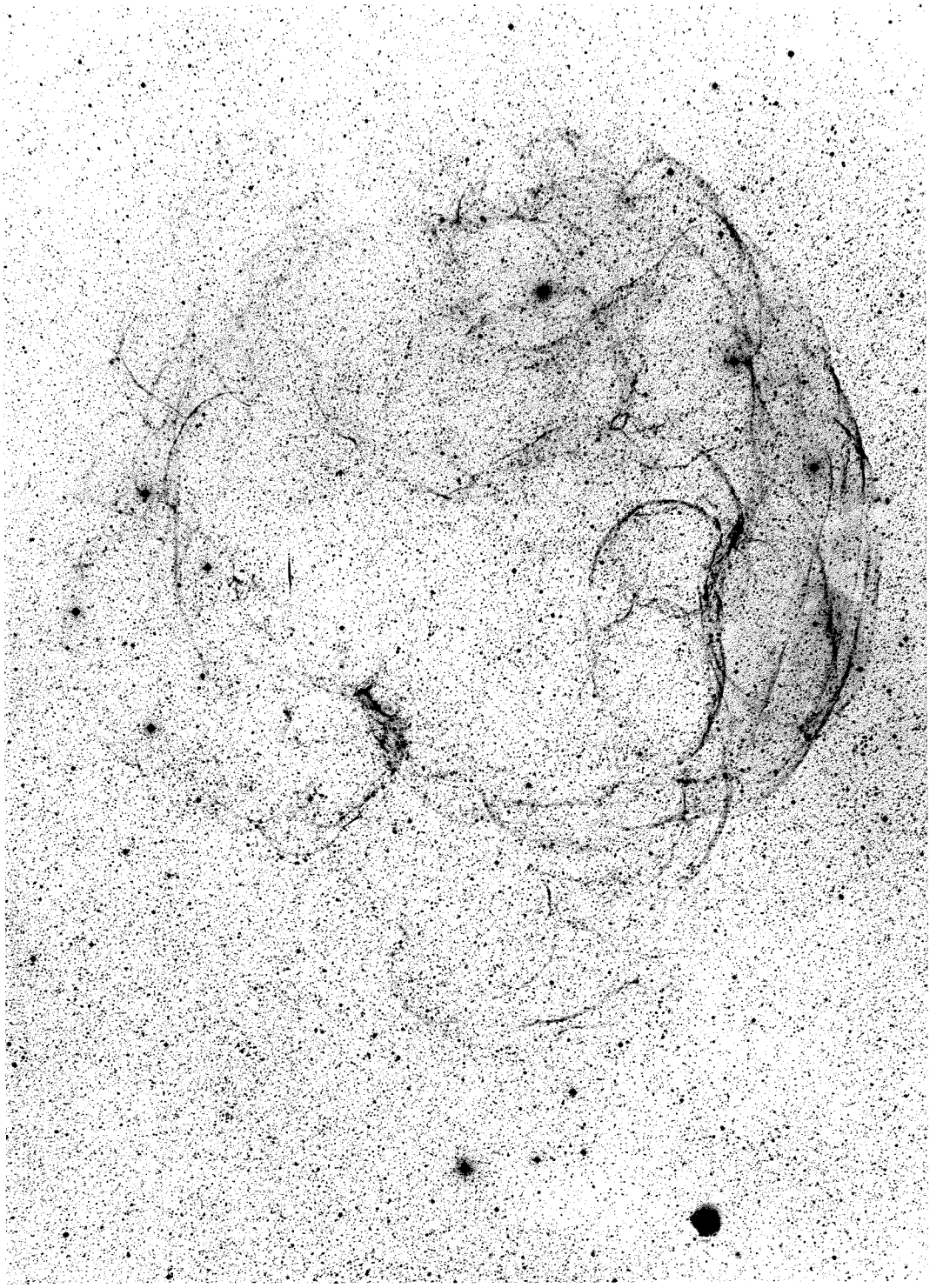

Figure 18 Photograph of S147.

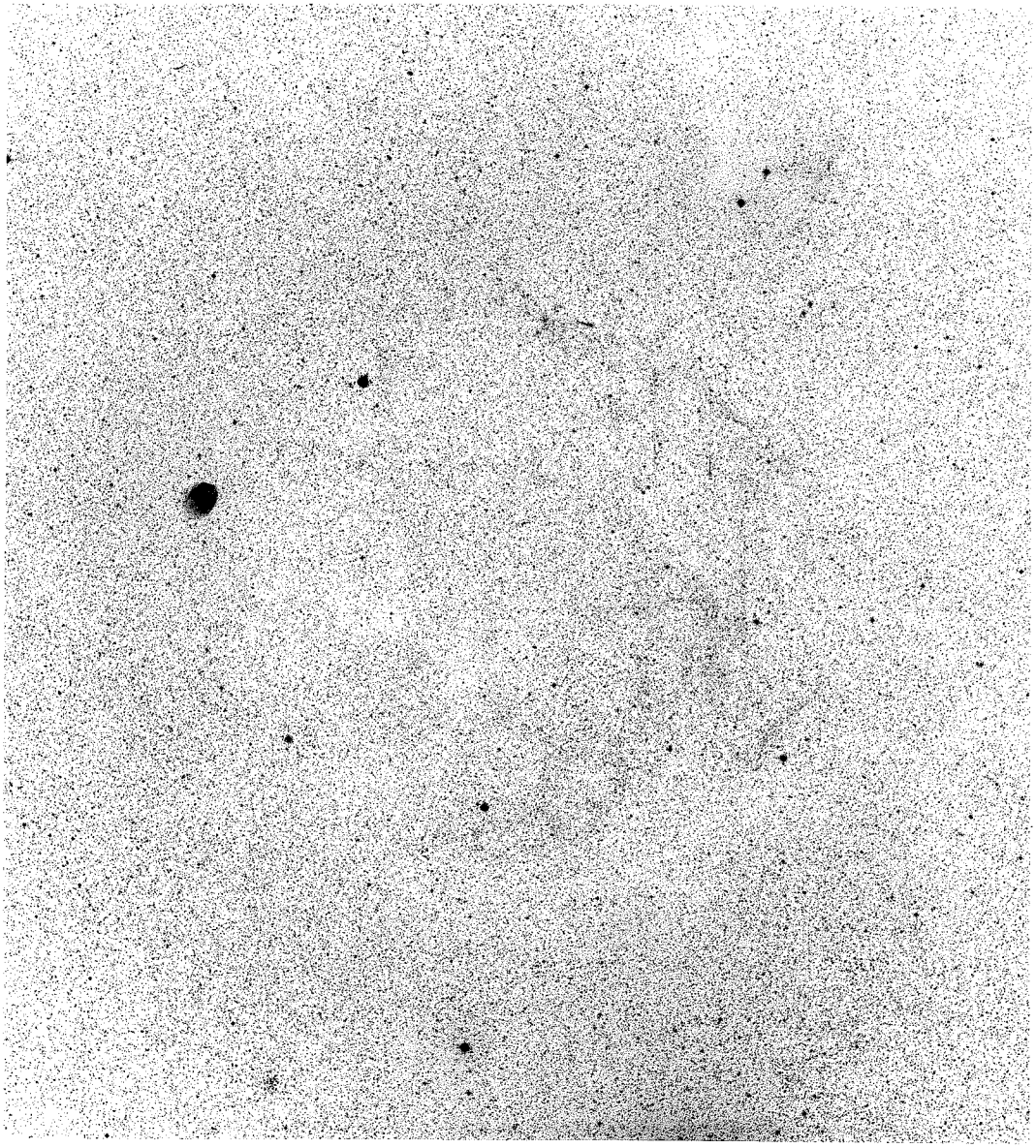

Figure 19 Photograph of HB9.

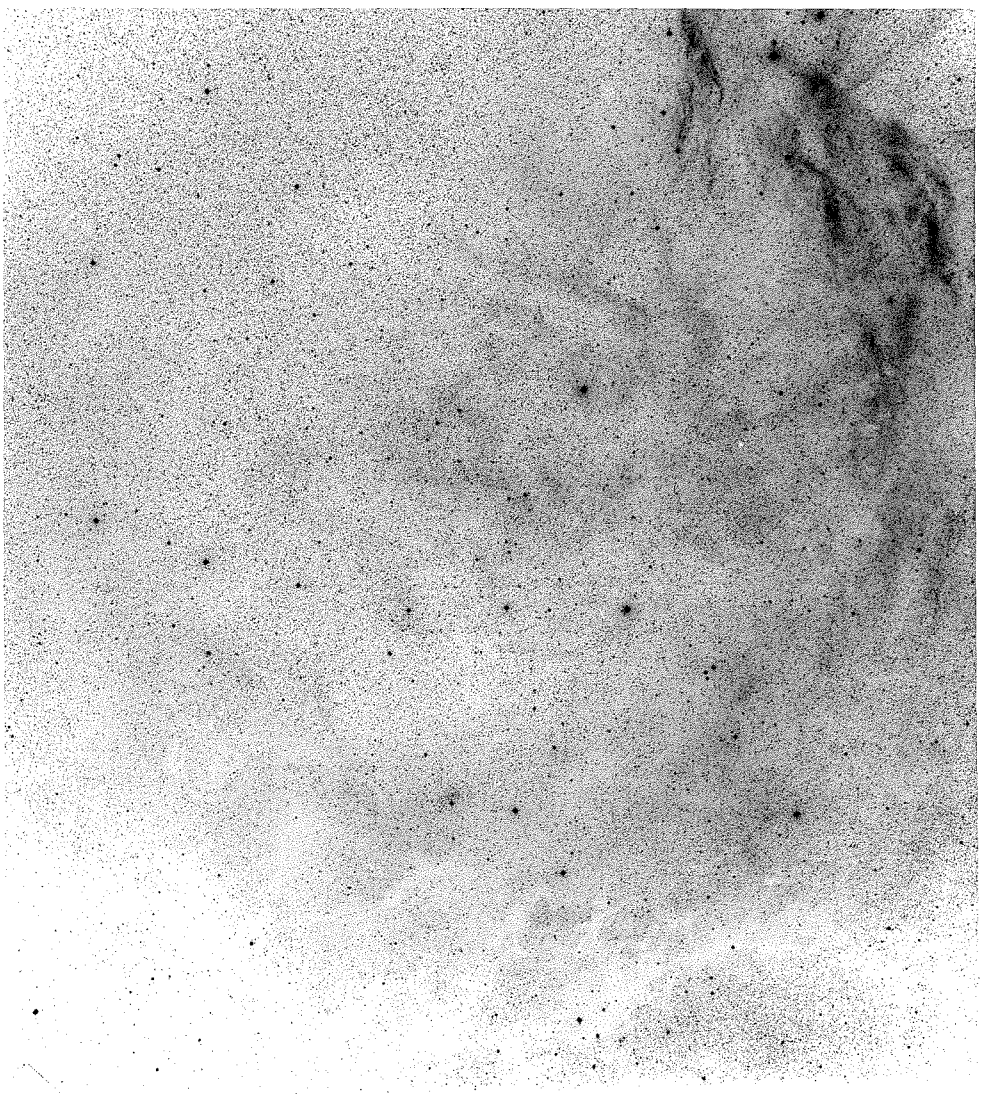

Figure 20 Photograph of HB21. The prominent emission in the lower right is not associated with the source.

References

Abell, G. 1960, Private Communication.

Allen, C. W. 1955, Astrophysical Quantities, (London: The Athlone Press).

Aller, L. H. 1956, Gaseous Nebulae, (New York: John Wiley and Sons Inc.).

Baade, W. 1943, Ap. J., 97, 119.

Baade, W. 1945, Ap. J., 102, 309.

Baade, W. 1956, B. A. N., XII, 312.

Baker, J. G., and Menzel, D. H. 1938, Ap. J., 88, 52.

Baldwin, J. E. 1955, M. N., 115, 690.

Baldwin, J. E., and Leslie, P. R. R. 1960, M. N., 120, 72.

Barat, J., Lequeux, J., and LeRoux, E. 1960, Comptes Rendus, 251, 2476.

Biraud, F., Lequeux, J., and LeRoux, E. 1960, Obs., 80, 116.

Bok, B. J. and Warwick, C. 1957, A. J., 62, 323.

Bolton, J. G., Stanley, G. J., and Slee, O. B. 1954, A. J. P., 7, 110.

Brown, R. H., Davies, R. D., and Hazard, C. 1960, Obs., 80, 191.

Brown, R. H., and Hazard, C. 1953, M. N., 113, 123.

Burbidge, E. M. and Burbidge, G. R. 1959, Paris Symposium on Radio Astronomy, ed. R. N. Bracewell, (Stanford: Stanford University Press), p. 323.

Burgess, A. 1958, M. N., 118, 477.

Chamberlain, J. W. 1953a, Ap. J., 117, 387.

Chamberlain, J. W. 1953b, Ap. J., 117, 399.

Eaton, J. J., and Kraus, J. D. 1959, Ap. J., 129, 284.

Edge, D. O., Shakeshaft, J. R., McAdam, W. B., Baldwin, J. E., and Archer, S. 1959, Mem. R. A. S., 68, 37.

Elsmore, B., Ryle, M., and Leslie, P. R. R. 1959, Mem. R. A. S., 68, 61.

Ginzburg, V. L. 1958, Progress in Elementary Particle and Cosmic Ray Physics. Volume IV, ed. by J. G. Wilson and S. A. Wouthuysen, (Amsterdam: North-Holland Publishing Company), p. 337.

Ginzburg, V. L. 1959, Paris Symposium on Radio Astronomy, ed. R. N. Bracewell, (Stanford: Stanford University Press), p. 589.

Gold, T., and Hoyle, F. 1959, Paris Symposium on Radio Astronomy, ed. R. N. Bracewell, (Stanford: Stanford University Press), p. 583.

Goldstein, S. 1960, Paper read to the Mexico Meeting of the American Astronomical Society.

Haddock, F. T., Mayer, C. H., and Sloanaker, R. M. 1954, Nature, 174, 176.

Hagen, J. P., Lilley, A. E., and McClain, E. F. 1955, Ap. J., 122, 361.

Hoyle, F. 1960, M. N., 120, 338.

Kellermann, K. I., and Harris, D. E. 1960, Obs. of the Calif. Inst. Tech. Radio Obs., No. 7.

Leslie, P. R. R. 1960, Obs., 80, 23.

Mathewson, D. S., Large, M. I., and Haslam, C. G. T. 1961, M. N., 121, 543.

Mayer, C. H., McCullough, T. P., and Sloanaker, R. N. 1957, Ap. J., 126, 468.

McGee, R. X., Slee, O. B., and Stanley, G. J. 1955, A. J. P., 8, 347.

Mills, B. Y., and Slee, O. B. 1957, A. J. P., 10, 162.

Mills, B. Y., Slee, O. B., and Hill, E. R. 1958, A. J. P., 11, 360.

Mills, B. Y., Slee, O. B., and Hill, E. R. 1960, A. J. P., 13, 676.

Minkowski, R. 1958, Rev. Mod. Phys., 30, 1048.

Minkowski, R. 1959, Paris Symposium on Radio Astronomy, ed. R. N. Bracewell, (Stanford: Stanford University Press), p. 315.

Moffet, A. T. 1960, Private Communication.

Oort, J. H., and Walraven, Th. 1956, B. A. N. XII, 285.

Opik, E. J. 1953, Irish A. J., 2, 219.

Osterbrock, D. E. 1958, Pub. A. S. P., 70, 180.

Osterbrock, D. E., and Stockhausen, R. E. 1960, Ap. J., 131, 310.

Piddington, J. H., and Trent, G. H. 1956, A. J. P. 9, 74.

Radhakrishnan, V., and Roberts, J. A. 1960, Phys. Rev. Letters, 4, 493.

Rishbeth, H. 1956, A. J. P., 9, 494.

Rishbeth, H. 1958, A. J. P., 11, 550.

Seeger, C. L., Westerhout, G., and Conway, R. G. 1957, Ap. J., 126, 585.

Seeger, C. L., Westerhout, G., and Van de Hulst, H. C. 1956, B. A. N., XIII, 89.

Shakeshaft, J. R., Ryle, M., Baldwin, J. E., Elsmore, B., and Thompson, J. H. 1955, Mem. R. A. S., 67, 106.

Sheridan, K. V. 1958, A. J. P., 11, 400.

Shklovsky, I. S. 1960a, Soviet Astronomy, 4, 243.

Shklovsky, I. S. 1960b, Soviet Astronomy, 4, 355.

Van den Bergh, S. 1960, Zeit. für Astrophysik, 51, 15.

Walsh, D., and Brown, R. H. 1955, Nature, 175, 808.

Westerhout, G. 1956, B. A. N., XII, 309.

Westerhout, G. 1958, B. A. N., XIV, 215.

Westerhout, G. 1960, Private Communication.

Whitfield, G. R. 1957, M. N., 117, 680.

Whitfield, G. R. 1960, M. N., 120, 581.

Wilson, R. W., and Bolton, J. G. 1960, Pub. A. S. P., 72, 331.

Woltjer, L. 1958, B. A. N., 14, 39.